TRPM4 Expression as a Predictive Biomarker and a Mechanistic Driver of Acetalax Activity in Prostate Cancer: Preclinical Efficacy Studies

Yuka Hoshi-Kadonosawa[1§], William C, Reinhold[1§], Daiki Taniyama[1], Yoshitaka Inoue[3,4], Augustin Luna[1,3], Suresh Kumar[1], Nai-Yun Sun[1,2], Yoo Sun Kim[1], Juanjuan Yin[5], Nitin Roper[1], Adam G. Sowalsky[5], William D. Figg[5], Naoko Takebe[1,2§§*], Yves Pommier[1§§*]

[1] Developmental Therapeutics Branch, Center for Cancer Research, National Cancer Institute, National Institutes of Health, Bethesda, MD, USA
[2] Stephenson Cancer Center, the University of Oklahoma, OK, USA
[3] Library of Medicine, National Institutes of Health, Bethesda, MD, USA
[4] Department of Computer Science and Engineering, College of Science and Engineering, University of Minnesota, Minneapolis, MN, USA
[5] Genitourinary Malignancies Branch, National Cancer Institute, Bethesda, MD, USA

[§] Co-first authors.
[§§] Co-senior authors
* Corresponding authors

Running Title: TRPM4 as a Biomarker of Acetalax Sensitivity

Keywords: TRPM4, Acetalax, Drug Repurposing, Prostate Cancer, Oncosis, Cell Swelling, Biomarker, Therapeutics, Patient-derived xenograft

Corresponding Authors:
1) Yves Pommier, Developmental Therapeutics Branch, CCR/NCI, NIH. Building 37, Room 5068 Bethesda, MD 20892-4255, USA
Phone: 240-760-6142
E-mail: pommier@nih.gov
2) William Reinhold, Developmental Therapeutics Branch, CCR/NCI, NIH. Building 37, Room 5041 Bethesda, MD 20892-4255, USA
Phone: 240-760-7339
E-mail: wcr@mail.nih.gov
3) Naoko Takebe Stephenson Cancer Center, University of Oklahoma 800 NE 10th Street Oklahoma City, OK 73104. USA Phone: 405-593-4105
E-mail: Naoko-takebe@ou.edu

Financial Support:
This work was supported by the Intramural Research Program of the National Cancer Institute, National Institutes of Health. This research was also supported in part by the Intramural Research Program of the National Institutes of Health (NIH) (ZIALM240126). The contributions of the NIH author(s) are considered Works of the United States Government. The findings and conclusions presented in this paper are those of the author(s) and do not necessarily reflect the views of the NIH or the U.S. Department of Health and Human Services.
The authors declare no potential conflicts of interest.

Abstract

Background: Advanced and treatment-refractory prostate cancer, including castration-resistant disease, require new therapeutic strategies. TRPM4, a calcium-activated monovalent cation channel, regulates cell volume and promotes cancer progression. Acetalax induces oncosis-like death in TRPM4-positive triple-negative breast cancers, suggesting a TRPM4-dependent vulnerability. Here, we investigated whether TRPM4 expression defines Acetalax sensitivity in prostate cancer.
Methods: We compared Acetalax sensitivity in TRPM4-high and -low prostate cancer cell lines, including androgen-dependent (LNCaP), castration-resistant (22Rv1), and androgen-independent (PC3, DU145) models. We evaluated TRPM4 dynamics and oncosis-associated phenotypes by Western blotting and immunofluorescence. Resistant clones were developed through continuous drug exposure. TRPM4 expression in patient samples was analyzed using prostate cancer tissue microarray and The Cancer Genome Atlas (TCGA). Transcriptional changes following TRPM4 loss were examined by RNA sequencing (RNA-seq). Antitumor activity and tolerability were evaluated in TRPM4-positive patient-derived xenograft (PDX) models.
Results: TRPM4-high cells (PC3, LNCaP and 22Rv1) underwent oncosis-like swelling and TRPM4 degradation upon Acetalax exposure, whereas TRPM4-low cell and resistant clones (DU145 and chronic exposure cells) remained insensitive and lacked TRPM4 expression. RNA-seq revealed transcriptomic remodeling associated with TRPM4 loss. TRPM4 was significantly elevated in tumors versus normal tissues and was unchanged across stages or Gleason scores. In TRPM4-positive PDX models, Acetalax (300 mg/kg) significantly suppressed tumor growth without body-weight loss, indicating antitumor efficacy without overt toxicity.
Conclusions: TRPM4 is a mechanistic driver and predictive biomarker of Acetalax response in prostate cancer, supporting TRPM4-dependent targeting and providing a rationale for the clinical development of Acetalax for TRPM4-expressing and treatment-refractory prostate cancer.

Significance

This study identifies TRPM4 as a mechanistic driver and predictive biomarker of Acetalax sensitivity in prostate cancer including castration-resistant disease, and demonstrates TRPM4-dependent antitumor efficacy *in vivo*, supporting its biomarker-guided clinical development.

Introduction

Prostate cancer remains the fifth leading cause of cancer death in men (1). While the prostate cancer treatment landscape continues to change with additional therapeutic options being introduced leading to an improved 5-year overall survival rate of 32% from 28% in 2013 (2), it needs further improvement. Androgen-deprivation therapy (ADT) is the mainstay for early-stage prostate cancer with initial responses above 80% (3). For advanced or metastatic prostate cancer, ADT is often combined with newer agents such as abiraterone plus prednisone, apalutamide or enzalutamide to improve outcomes (4) (5). Recently-approved targeted treatment for patients with specific genetic mutations include the PARP inhibitors olaparib, rucaparib and niraparib (5) (6) (7).

There are several indicators of worsening prognosis in patients with prostate cancer. One is castration-resistant androgen-independent growth following a failure of conventional treatments, often leading to subsequent metastatic spread (3). A second negative prognostic indicator is a high Gleason grade or score. Increasing scores are associated with increased mortality, increased chance of biochemical recurrence of prostate specific antigen (PSA) and metastatic progression (8) (9). A third negative prognostic indicator strongly associated with decreasing survival is increasing disease stage (9) (10).

Transient Receptor Potential Melastatin 4 (TRPM4) is a calcium-activated and voltage-dependent monovalent cation channel gene (11). It is overexpressed in both prostate cancer cell lines and patient samples (12). Upregulation of TRPM4 occurs during the transition from pre-cancerous prostatic intraepithelial neoplasia to prostate carcinoma (13). Biochemical recurrence risk (the increase of PSA levels after surgery) is associated with TRPM4 protein overexpression following radical prostatectomy (14). Androgen-independent prostate cancer progression, cancer cell migration and increased cell proliferation in prostate cancer are all proposed to be positively affected by TRPM4 overexpression (12) (15) (16) (11).

Oxyphenisatin Acetate (Acetalax) has been described as causing a starvation response, autophagy and mitochondrial dysfunction in breast cancer cell lines as well as having *in vivo* antiproliferative activity (17). Our group has studied Acetalax for repurposing as an anticancer agent for triple-negative breast cancer (TNBC) (18). Acetalax induces robust cytotoxicity in a subset of TNBC with morphological changes, increased cellular permeability, decreased mitochondrial membrane potential, increased ATP depletion and increased mitochondrial fragmentation (19). We showed that Acetalax is a distinct class of drug with a novel mechanism of action discovered through bioinformatics and hierarchical clustering analyses as compared with 58 FDA-approved or 58 clinical trial drugs (20). *In vivo*, Acetalax is efficacious with no obvious side effect, and it penetrates tumors (20).

TRPM4 protein is present on the cell membrane of Acetalax-sensitive while being absent in Acetalax-resistant TNBC cell lines (19). Knockout of TRPM4 leads to Acetalax-resistance and knock-in to Acetalax-sensitivity, demonstrating causality for TRPM4 regarding Acetalax activity as a potent agonist of TRPM4 (19). Supportively, in

multivariate analysis, TRPM4 transcript levels are a top predictor of Acetalax activity (20). Acetalax also causes proteasome-dependent TRPM4 protein degradation (20).

In this study, we demonstrate that TRPM4 expression determines sensitivity to Acetalax in prostate cancer. Using isogenic TRPM4-positive and TRPM4-negative models, we show that Acetalax induces oncosis-like cell death selectively in TRPM4-expressing cells. Furthermore, TRPM4 degradation following Acetalax treatment is observed across *in vitro* and *in vivo* models. Through transcriptomic analyses, we identify TRPM4 loss-associated transcriptomic remodeling in Acetalax-resistant cells. Importantly, *in vivo* validation using TRPM4-expressing prostate cancer patient-derived xenograft (PDX) models confirms that Acetalax significantly suppresses tumor growth, consistent with our *in vitro* observations.

We show that TRPM4 expression is associated with clinical parameters such as Gleason score and tumor stage using The Cancer Genome Atlas (TCGA) and tissue microarray cohorts, supporting TRPM4's role as a potential prognostic biomarker. Together, our findings establish TRPM4 as both a primary target of Acetalax and a clinically relevant biomarker in prostate cancer, providing a rationale for repurposing Acetalax as a targeted therapy for TRPM4-expressing prostate tumors.

Materials and Methods

Patient transcript level bar plot

The normal versus tumor bar plot was created using Gene Expression Profiling Interactive Analysis (GEPIA2, http://gepia2.cancer-pku.cn/#general, RRID:SCR_026154).

Scatter plots

The TRPM4 versus FOLH1 and KLK3 scatter plots for 8 CCLE prostate cell lines was done using the Genomics and Pharmacology facility (RRID:SCR_025664) CellMinerCDB (https://discover.nci.nih.gov/rsconnect/cellminercdb/, RRID:SCR_025640) using "Univariate Analysis\ Plot Data" tabs choosing "Select Tissues \ To include \ Prostate" to limit the cell lines (21). The Acetalax activity data versus TRPM4 scatter plot for 6 GDSC prostate cell lines was done using CellMinerCDB using "Univariate Analysis\ Plot Data" tabs choosing "Select Tissues \ To include \ Prostate" to limit the cell lines (21).

Analysis of TRPM4 expression in TCGA-PRAD and Stand up to cancer (SU2C) metastatic castration-resistant prostate cancer (mCRPC) datasets

Publicly available RNA-seq datasets were analyzed to evaluate the relationship between TRPM4 expression and androgen receptor (AR)– and neuroendocrine (NE)–associated gene signatures in clinical prostate cancer samples. For primary prostate cancer, RNA-seq expression data (TPM) from the TCGA Prostate Adenocarcinoma (TCGA-PRAD) cohort were analyzed. For metastatic disease, RNA-seq expression data

(RPKM) from the SU2C/PCF Dream Team metastatic castration-resistant prostate cancer (mCRPC) cohort (Cell 2015) were used. Spearman rank correlation coefficients were calculated to assess the association between TRPM4 expression and representative AR-associated genes and NE-associated genes.

To classify tumors based on their NE status, their scores were calculated as the mean expression of *CHGA, SYP, ASCL1,* and *INSM1*. Tumors in the top quartile of AR score and bottom quartile of NE score were classified as *AR-high/NE-low*, whereas tumors in the bottom quartile of AR score and top quartile of NE score were classified as *AR-low/NE-high*. Differences in TRPM4 expression between groups were assessed using the Wilcoxon rank-sum test. All statistical tests were two-sided.

Cell lines and Reagents

Human prostate cancer cell lines, PC3 (RRID: CVCL_0035), LNCaP (RRID: CVCL_0395) and 22Rv1 (RRID: CVCL_1045) were obtained from ATCC (American Type Culture Collection) and authenticated by STR profiling (Laragen) every six months. The DU145 (RRID: CVCL_0105) cell line was obtained from the Developmental Therapeutics Program (DTP). The DTP has its own internal authentication, and we did not duplicate this. PC3 cells were grown in F-12 medium (Thermo Fisher Scientific) containing 10% fetal bovine serum (GeminiBio) and 1% penicillin/streptomycin (Gibco). LNCaP and 22Rv1 cells were cultured in RPMI medium (Thermo Fisher Scientific) containing 10% fetal bovine serum (FBS) (GeminiBio) and 1% penicillin/streptomycin (Gibco). DU145 cells were grown in DMEM medium (Thermo Fisher Scientific) containing 10% fetal bovine serum (GeminiBio) and 1% penicillin/streptomycin (Gibco). Cells were cultured at 37 ^{0}C in 5% CO2 incubator. Cells were monitored for mycoplasma negativity with MycoAlert Mycoplasma Detection Kit (Lonza). Acetalax (NSC 59687) and Bortezomib (BTZ) were obtained from NCI DTP (DCTD, NCI, NIH) (RRID:SCR_003057).

Cell viability assay

Cell plating was done in 384-well plates at a density of 300 cells/well in 30 µL medium and allowed to grow for 24 h. The cells were then treated with Acetalax as described (see figure and figure legends for details). At 72 h treatment, cell viability was measured using the ATPlite 1-step Luminescence Assay System (PerkinElmer, Waltham, MA, USA) using a luminescence plate reader. Viability plots were generated and the data analyzed using GraphPad Prism 10 software (GraphPad Software Inc, RRID:SCR005375) Experiments were performed in triplicate (n=3).

Immunofluorescence microscopy

Cells were plated on 24x60 mm sized microscope cover glasses in an 8-well plate at a density of 1 $\times 10^5$ cells/well in 500 µl complete medium. After 24 h, cells were treated with Acetalax as described in the figure legends. After washing with PBS, cells were fixed in 4% paraformaldehyde (PFA) and permeabilized with 0.5% Triton X-100/PBS and blocked with 3% bovine serum albumin (BSA)/PBS-T for 1 hour. Cells were stained with anti-TRPM4 antibody [OTI10H5] (ab123936, Abcam, RRID: AB_10976061) (1:250 dilution) PBS-T overnight at 4℃. After washing with PBS, cells were incubated with Alexa Fluor 488 Phalloidin antibody (A12379, Invitrogen) (1:200 dilution) PBS-T, and Alexa Fluor 568 secondary antibody (1:1,000 dilution) for 1 hour at room temperature. After that, cells were incubated with DAPI (62248, Thermos Scientific) (1:1000 dilution) for 30 minutes and mounted with ProLong Glass Antifade Mountant (P36980, Invitrogen) on cover slides. Images were taken with a Zeiss Axio Observer microscope (Carl Zeiss Microscopy GmbH) equipped with an Apotome 3 structured illumination *module and a Plan-Apochromat 63×/1.4 NA oil immersion objective.* Fluorescence intensity was quantified for TRPM4 degradation using ImageJ2 software (version 2.14, RRID:SCR_003070). PC3 cells stained with Alexa Fluor 488-labeled secondary antibodies against TRPM4 were imaged, and the green channel was used for analysis. Approximately 80–100 cells were analyzed per condition. The quantitation results of the fluorescence intensity were visualized using GraphPad Prism 10.

Analysis of cell and nuclear size & membrane blebbing frequency

Analyses of cell and nucleus size and bleb frequency were carried out by assessing photographs taken under identical conditions with a Zeiss Axio Observer microscope (RRID:SCR_023692). Arbitrary locations containing 2 to 40 cells per field were chosen for photography using a 63× objective lens. Size was assessed by reading with ImageJ2 (ver. 2.14) software. Cells with blebbing were counted manually. Protruding cells in the image were excluded from the analysis. Adherent cells were manually separated using Image J2 to measure the size of a single cell. Quantitation of cell swelling, nuclear swelling and blebbing was performed using GraphPad Prism 10.

Western blotting

Cell pellets were collected, added to PBS and treated with an equal volume of SDS buffer with a final concentration of 5% β-mercaptoethanol, and heated at 95°C for 5 minutes after sonication. Protein concentrations were determined by Bio-Rad Protein Assay Dye Reagent (Bio-Rad). Cell lysates were separated on reducing SDS-PAGE gels (Invitrogen) and transferred onto PVDF membranes (Millipore). Membranes were immunoblotted with the following antibodies: TRPM4 [OTI10H5] (ab123936, Abcam, RRID: AB_10976061) (1:1000 dilution), GAPDH [6C5] (sc-32233, Santa Cruz Biotechnology) (1:2000 dilution). Membranes were incubated overnight, with species-appropriate horseradish peroxidase (HRP)-conjugated secondary antibodies. ChemiDoc MP Imaging System (Bio-Rad) with SuperSignal™ Wset Pico PLUS or Ultimate Sensitivity Chemiluminescent Substrate (Thermo Scientific 34580 or A38555) were used to visualize the protein signals.

Densitometric analyses of immunoblot bands were performed using ImageJ2 with the Band/Peak Quantification Tool v1 macro (22). Equal-sized rectangular regions of

interest (ROIs) were applied to each lane, and background subtraction was performed using identical parameters. Integrated band intensities were quantified and normalized to the corresponding GAPDH signal for each sample. Normalized values were expressed relative to the control condition (control = 1).

TRPM4 knockdown and cell viability assay

TRPM4 knockdown (KD) was achieved in human prostate cancer PC3 cells using ON-TARGETplus SMARTpool siRNA targeting human TRPM4 (Horizon Discovery). For validation of knockdown efficiency, PC3 cells were seeded at 2.0 × 10^5 cells per well in 6-well plates and transfected the following day with TRPM4 siRNA (10 or 20 nM final concentration) or non-targeting control (NTC) siRNA using Lipofectamine RNAiMAX (Thermo Fisher Scientific) according to the manufacturer's instructions. TRPM4 protein reduction was confirmed by Western blot analysis 72 h after transfection.
For drug sensitivity assays, reverse transfection was performed in 96-well plates by adding siRNA–Lipofectamine complexes prior to cell seeding to achieve a final siRNA concentration of 20 nM. Cells were seeded at 1,000 cells per well in 100 µL complete growth medium and incubated for 72 h to allow TRPM4 depletion. Cells were then treated with Acetalax at the indicated concentrations by adding an equal volume of drug-containing medium and incubated for an additional 72 h. Cell viability was determined using the ATPlite assay as described above. Dose–response curves were generated using GraphPad Prism 10. Experiments were performed in technical triplicates.

Generation of Acetalax resistant cells

PC3 and LNCaP cells, which were originally sensitive and expressing TRPM4, were chronically exposed to Acetalax in a dose titration manner. A total of 3 x 10^5 cells were seeded in a 10-cm dish, and when the dish reached almost full confluency in 1 to 2 weeks, the cells were passaged with double the concentration of Acetalax. Acetalax concentration was initially set at 0.2 µM and increased in two-fold increments up to 12.8 µM. After that, the concentration was increased by 10 µM increments starting from 20 µM. When the concentration of Acetalax was increased to 60 µmol/L for PC3 cells and 50 µmol/L for LNCaP cells, cell proliferation was inhibited. Therefore, PC3 cells chronically exposed to 40 µmol/L Acetalax and LNCaP cells chronically exposed to 30 µmol/L Acetalax were designated as Acetalax chronically exposed (CE) cells, representing Acetalax-resistant cell derivatives. Prior to each experiment, CE cells were cultured in Acetalax-free medium for two weeks.

Immunohistochemistry, Tissue arrays

A prostate tissue array slide (TissueArray.Com, catalog #PR753a) was used to stain adenocarcinoma and benign hyperplasia samples. Immunohistochemistry (IHC) staining was conducted using the Bond RX autostainer (Leica Biosystems) under the following conditions: Epitope Retrieval 2 (EDTA) for 20 min, TRPM4 primary antibody (Abcam, #ab123936, RRID: AB_10976061) at 1:200 for 30 min. Detection used the Bond Polymer Refine Detection Kit (Leica Biosystems, #DS9800). As a negative control, an isotype-matched control reagent (mouse IgG2a, BD Biosciences, #553454) was

substituted for the primary antibody. Whole-slide imaging was performed at 20× magnification using the Aperio AT2 scanner (Leica Biosystems, Buffalo Grove, IL, USA, RRID:SCR_021256). Stained IHC slides were quantified using HALO image analysis software (version 3.6, Indica Labs, Albuquerque, NM, USA). Automated quantification of the percentage of positive immune cells per core was performed using the cytonuclear algorithm (V2.0.5).

Gene expression analysis using TCGA-PRAD and GTEX prostate data, Gleason score and disease Stage

RNA sequencing (RNA-seq) data and related clinical information for prostate adenocarcinoma (TCGA-PRAD, RRID:SCR_003193) and normal (prostate, GTEX, RRID:SCR_001618) were obtained from the UCSC Xena browser (https://xenabrowser.net/, RRID:SCR_018938). Gene expression levels were calculated based on log2-transformed TPM (transcripts per million) values. TRPM4 expression data were extracted and integrated with clinical annotations including Gleason grade, American Joint Committee on Cancer (**AJCC)** pathological TNM (tumor, node, metastasis) classification, and sample type (normal vs tumor) (23). Reconstructed stage information (Stage I/II, III, and IV) was derived from available T, N, and M categories according to the AJCC staging guidelines for prostate. Gleason score was derived from Gleason grade and was classified based on the primary Gleason patterns Grade 1–3 vs Grade 4–5 (23). TRPM4 expression differences were evaluated using the Wilcoxon rank-sum test for two-group comparisons. All statistical analyses and visualizations were performed using R version 4.3.2.

Comparison of prostate cancer cell lines and TCGA prostate adenocarcinomas

We compared approximately 500 prostate adenocarcinomas samples from the TCGA project to our four prostate cancer cell lines, 22Rv1, LNCaP-Clone-FGC, DU-145 and PC-3, using gene expression, copy number, and mutation data using TumorComparer (24).

RNA-seq

RNA-seq was performed on PC3 and LNCaP parental and CE cells that had been Acetalax-free for 2 weeks. RNA was extracted from a control group of these cells and from cells treated with Acetalax at 10 µmol/L for 4 hours per protocol using the RNeasy Mini Kit (Cat: NC9307831, Qiagen). For each condition, RNA extraction was performed in biological triplicates. The extracted RNA was measured for RNA quality (RIN) with the Agilent Tape Station System. We used 800 ng of total RNA samples to generate the library (PolyA selected). The kits used for the library preparation were the NEBNext Poly(A) mRNA Magnetic Isolation Module (E7490), NEBNext Ultra II Directional RNA Library Prep Kit for Illumina with Sample Purification beads (NEB #E7765), and NEBNext® Multiplex Oligos for Illumina® (96 Unique Dual Index Primer Pairs, NEB, E6440S) as described in the manufacturer's manual. Sequencing was carried out on the NextSeq 2000 (RRID:SCR_023614) instrument with the NextSeq 1000/2000 XLEAP-SBS P3 200 cycle kit, paired-end 100x100 (Illumina, Cat# 20100989). Demultiplexing

was carried out with the illumina DRAGEN BCL convert software version 4.2.7. The Gene Expression Omnibus repository accession number is GSE313554.

Bioinformatic analyses

RNA-seq fastq files were processed using the RENEE pipeline (25), which performs quality control, alignment to the hg38 reference genome with STAR (26), and expression quantification with RSEM. Count matrices generated by the pipeline were used for downstream analyses. Genes with zero counts across both conditions were excluded. Expression values were then transformed as log2(FPKM + 1) to stabilize variance. For each gene, we calculated a score as the difference in mean expression between treatment and control samples. To further examine baseline differences, comparisons were also performed between control groups (PC3 vs PC3-CE, LNCaP vs LNCaP-CE). Genes were ranked according to these scores, whereas positive values indicated upregulation and negative values indicated downregulation. Gene set enrichment analysis was carried out with the GSEApy Python package, using hallmark gene sets (27), EMT signatures (28), immediate early response genes (29), and immune-related signatures (30).

TRPM4 correlation analyses

To investigate transcriptional programs associated with TRPM4, we used the $\log_2$-transformed FPKM values generated by the RENEE/RSEM pipeline (described above). Gene symbols were deduplicated by retaining the isoform with the highest mean expression. Pearson correlation coefficients were calculated between TRPM4 expression and all other genes across the full RNA-seq dataset, including PC3 and LNCaP parental and CE samples, with and without short-term exposure. Genes were ranked according to their correlation coefficients in descending (positive) or ascending (negative) order, and genes absent from the filtered expression matrix were excluded. For downstream visualization, the top 20 positively correlated and top 20 negatively correlated genes were selected. TRPM4 was optionally included as an internal reference to illustrate relative expression patterns.

Heatmap visualization

Heatmaps were generated in R using the heatmap package (v4.5.1). For each selected gene, expression values were standardized across samples using z-score transformation after $\log_2$(FPKM + 1) normalization. Columns were grouped into four biological categories: PC3-Parental, PC3-CE, LNCaP-Parental, and LNCaP-CE. Unless otherwise indicated, only control-treated samples were used in the heatmaps to visualize baseline transcriptomic differences independent of drug exposure. Sample-level annotations, including cell line identity and CE status, were displayed using color-coded sidebars. When included, TRPM4 was positioned at the top of the heatmap to serve as a reference marker for correlated gene clusters.

Patient-Derived Xenograft (PDX) studies

The *in vivo* efficacy of Acetalax was evaluated in prostate cancer patient-derived xenograft tissues LuCaP147, castration-sensitive and LuCaP167, castration-resistant).

The study design and animal use were approved by the NCI-Bethesda Animal Care and Use Committee (IACUC number: DTB-007). We used 6- to 8-week-old male NOD-*scid* IL2Rgamma^{null} [NSG] mice injected subcutaneously into the right flank with 4 × 10^6 single cells prepared from established PDX tumors (LuCaP147 and LuCaP167) following mechanical and enzymatic dissociation (in HBSS/Matrigel). One week later, after tumors became observable, mice were started on Acetalax 100 mg/Kg or 300 mg/kg daily (Monday to Friday) using intraperitoneal injection. The placebo mice were treated with saline (n=5 per group). Mouse body weight and tumor volume were measured twice a week, and tumor volume was calculated by measuring the length (L) and width (W) of the tumor with calipers and using the formula ($L \times W^2$)/2. Tumor volumes and body weights were measured at the indicated time points during the treatment period. To evaluate overall changes throughout the study, the area under the curve (AUC) for each individual tumor growth curve and body weight trajectory was calculated using the trapezoidal rule in GraphPad Prism 10. The resulting AUC values were used as summary measures and compared among treatment groups using the Kruskal–Wallis test followed by Dunn's multiple comparisons test. A p value < 0.05 was considered statistically significant.

Immunohistochemistry, cell lines and PDX tissues

Formalin-fixed paraffin-embedded (FFPE) sections prepared from PC3 and DU145 cells, either untreated (Control) or treated with 10 µmol/L Acetalax for 4 hours, as well as FFPE sections from prostate cancer PDX tissues, were used for TRPM4 IHC. Optimized staining protocol included antigen retrieval performed by microwave heating in Antigen Retrieval Buffer (pH 6.0) (#ab93678, Abcam) for 20 min. The sections were incubated with mouse monoclonal anti-TRPM4 antibody (Abcam, #ab123936, 1:200, incubated for 30 min in TBST (1×TBS + 0.5% Tween 20)) overnight at 4 ℃. The sections were then incubated for 30 minutes in N-histofine Simple Stain MAX PO (MULTI) (Nichirei Biosciences Inc., #NIC-414151F) followed by 5 minutes incubation with chromogen DAB-3S (original dilution by manufacturer, Nichirei Biosciences Inc.; #415192F) at room temperature. Consensus regarding interpretation was made when there were discordant results.

Data Availability

RNA sequencing data generated in this study have been deposited in the Gene Expression Omnibus under accession number GSE313554. The dataset is currently under embargo and accessible to reviewers using the tokens provided. The data will be publicly available upon publication. All other data supporting the findings of this study are available within the article and its supplementary materials.

Results

TRPM4 is highly expressed in prostate cancer, and its expression is correlated with prostate lineage markers

Analysis of TRPM4 transcripts across 31 human tissues revealed a wide range of expression, with prostate showing the highest levels in both normal and tumor samples

(Figure 1A). Among all tissue types, prostate exhibits the most pronounced increase in TRPM4 from normal to tumor tissue, suggesting a prostate-enriched and cancer-associated pattern of expression. Correlation analysis using CCLE RNA-seq data demonstrates that TRPM4 expression is significantly associated with the prostate lineage markers FOLH1 (PSMA) and KLK3 (PSA) (Figure 1B–C). In contrast, TRPM4 is not significantly correlated with AR transcript levels (p = 0.073), indicating that TRPM4 expression is not dependent on androgen receptor signaling. These findings are consistent with TCGA analyses demonstrating elevated TRPM4 expression in prostate tumors compared to normal tissues (below section).

To assess the functional relevance of TRPM4 in this context, we evaluated Acetalax sensitivity across four prostate cancer cell lines with various androgen expression. Western blotting confirmed that TRPM4 protein is abundantly expressed in Acetalax-sensitive prostate cancer cell lines (LNCaP, PC3, and 22Rv1) whereas DU145 cells exhibit minimal TRPM4 expression (Figure 1D), consistent with their relative TRPM4 expression levels across the cell lines. LNCaP (androgen sensitive), PC3 (androgen independent) and 22Rv1 (castration-resistant)—each exhibiting relatively high TRPM4 transcript levels—showed strong sensitivity to Acetalax, whereas DU145, characterized by low TRPM4 expression, displayed marked resistance (Figure 1E). Consistent with these findings, TRPM4 transcript levels showed a strong positive correlation with Acetalax sensitivity across the prostate cancer cell lines in the GDSC dataset (Figure 1F), supporting TRPM4 as a key contributor to Acetalax responsiveness. These findings indicate that TRPM4 expression may serve as a potential determinant of Acetalax responsiveness in all stages of prostate cancer.

TRPM4 shows context-dependent association with AR and NE lineage markers in clinical prostate cancer datasets

In the TCGA-PRAD cohort, TRPM4 expression shows no significant correlation with AR expression (Spearman R = 0.014, $P = 0.75$) and only a weak negative correlation with the NE marker *CHGA* (Spearman R = −0.20, $P = 1.3 \times 10^{-6}$) (Supplemental Figure 1 and Supplemental Table 1). TRPM4 expression does not differ between AR-high/NE-low and AR-low/NE-high primary tumors ($P = 0.85$, Wilcoxon rank-sum test).
In the SU2C mCRPC cohort, TRPM4 expression was positively correlated with AR signaling genes (Spearman R = 0.33–0.40, P < 0.001) and negatively correlated with NE-associated genes (Spearman R = −0.20 to −0.27, P < 0.05) (Supplemental Figure 2 and Supplemental Table 2). TRPM4 expression was significantly higher in AR-high/NE-low tumors compared with AR-low/NE-high tumors ($P = 2.6 \times 10^{-5}$, Wilcoxon rank-sum test).

Acetalax induces morphologic changes consistent with oncosis

As we observed in the TNBC cell lines (20), Acetalax triggered rapid morphologic changes characteristic of oncosis in TRPM4-high prostate cancer cells (PC3). These changes progressed over time and were consistently observed across imaging and quantitative analyses (Figure 2A-B). By contrast, TRPM4-low DU145 cells showed no detectable alterations in cell size, nuclear morphology, or membrane integrity under identical treatment conditions (Figure 2C-D). Together, these results demonstrate that

Acetalax induces a TRPM4-dependent oncosis-like response distinguishing sensitive from resistant prostate cancer cells. We obtained similar results in 22Rv1, LNCaP and PC3 regarding significant cellular and nuclear swelling and cellular blebbing (Supplemental Figure 3A-D). Thus, sensitive prostate cancer cell lines exhibit early cell swelling, nuclear enlargement, and prominent membrane blebbing within minutes of exposure to Acetalax.

Acetalax induces TRPM4 degradation via the ubiquitin–proteasome system

To directly test whether TRPM4 determines Acetalax sensitivity, we performed siRNA-mediated knockdown of TRPM4 in PC3 cells. The knockdown efficiently reduced TRPM4 protein levels and significantly decreased cellular sensitivity to Acetalax compared with control cells (Figure 3A), indicating that TRPM4 expression contributes to the cytotoxic response to Acetalax. These findings provide functional evidence that TRPM4 expression contributes to Acetalax responsiveness in prostate cancer cells, indicating that TRPM4 levels contribute to Acetalax responsiveness in prostate cancer cells. In PC3 cells, Acetalax treatment resulted in a time-dependent reduction of TRPM4 protein levels, whereas GAPDH remained unchanged (Figure 3B).

Immunohistochemistry and immunofluorescence further demonstrated robust TRPM4 staining in untreated PC3 cells, which was markedly diminished following Acetalax exposure, consistent with rapid loss of TRPM4 protein (Figure 3C). In contrast, DU145 cells exhibited minimal TRPM4 staining regardless of treatment (Figure 3C), supporting its consistently low baseline TRPM4 expression and Acetalax resistance.

To determine the mechanism underlying TRPM4 loss, we evaluated the effect of proteasome inhibition. Co-treatment with bortezomib (0.5 μM) and Acetalax effectively rescued Acetalax-induced TRPM4 degradation, as demonstrated by both immunofluorescence and Western blotting (Figure 3D–E). Quantification of fluorescence intensity confirmed significant preservation of TRPM4 signal with bortezomib co-treatment (Figure 3D). Consistently, quantification of TRPM4 protein levels normalized to GAPDH from three independent Western blot experiments confirmed that bortezomib co-treatment prevented Acetalax-induced TRPM4 degradation (Figure 3E) while bortezomib treatment alone showed a modest and variable effect on TRPM4 levels. These findings imply that Acetalax promotes TRPM4 degradation through the ubiquitin–proteasome pathway, and that resistant cells lack TRPM4 irrespective of drug exposure.

Chronic Acetalax exposure generates resistant clones with TRPM4 loss

To elucidate the mechanisms of acquired resistance to Acetalax, we developed chronic exposure (CE) clones of PC3 and LNCaP cells (Figure 4A). These CE clones displayed a rightward shift in their Acetalax dose–response curve, consistent with resistance (Figure 4B). Notably, they also showed complete loss of TRPM4 (Figure 4C) while GAPDH levels were largely unchanged across conditions. Morphologically, parental cells exhibited cell and nuclear swelling and membrane blebbing rapidly after drug exposure, whereas CE cells remained unaffected (Figure 4D-E). These findings demonstrate that loss of TRPM4 is a hallmark of acquired resistance.

To evaluate the relevance of the prostate cancer models used in this study, we assessed how closely each cell line resembles human prostate tumors using TumorComparer (https://github.com/sanderlab/tumorcomparer). Across DNA copy-number aberrations, somatic mutations, and transcript expression, PC3, LNCaP, and 22Rv1 showed higher weighted similarity to patient tumors compared with DU145 (Supplemental Figure 4). These data support the suitability of the TRPM4-high, Acetalax-sensitive models as representative *in vitro* systems and underscore the distinct biology of DU145.

RNA-seq reveals transcriptomic reprogramming associated with TRPM4 loss

To further characterize the resistant phenotype, we performed RNA-seq in parental cells with or without short-term Acetalax treatment and in chronic-exposure (CE) cells. TRPM4 transcript levels were reduced in the CE clones relative to parental cells in both the PC3 and LNCaP backgrounds, consistent with the loss of TRPM4 protein (Figure 5A). Gene set enrichment analysis (GSEA) revealed coordinated transcriptomic remodeling in CE cells. Several oncogenic pathways were commonly upregulated in both PC3 and LNCaP CE clones, including E2F targets, G2/M checkpoint, MYC signaling, DNA repair and mitotic spindle programs (Figure 5B). Conversely, pathways downregulated in both CE lines included TNFα/NF-κB signaling, IL6/JAK/STAT3 signaling, EMT, hypoxia, and xenobiotic metabolism, indicating suppression of stress-response and inflammatory programs (Figure 5B).

To delineate gene networks associated with TRPM4 status, we performed correlation analyses using TRPM4 expression and global transcriptomic profiles. The top TRPM4-correlated genes included membrane-associated and metabolic regulators (e.g., *OSBPL5, CYB561, GLUL*) whereas negatively correlated genes were enriched for DNA repair, signaling regulators and tumor suppressors (e.g., *NHEJ1, ING1, FOXN2*) (Figure 5C; Supplemental Table 3). Heatmap visualization demonstrated separation of the TRPM4-expressing parental cells from the TRPM4-deficient CE clones both in the PC3 and LNCaP backgrounds (Figure 5C). Collectively, these findings indicate that TRPM4 loss drives a distinct transcriptional state characterized by enhanced proliferative and cell-cycle programs and reduced stress/inflammatory signaling, defining a molecular signature associated with Acetalax resistance.

Acute Acetalax treatment induced rapid TRPM4 degradation via the ubiquitin–proteasome pathway, as shown by proteasome inhibition experiments. In contrast, transcriptomic changes observed in CE cells reflected an adapted state associated with sustained TRPM4 loss. Consistent with this, pathway analysis of acute Acetalax exposure showed enrichment of stress and inflammatory signaling pathways and suppression of proliferative programs (Supplemental Figure 5).

Acetalax suppresses tumor growth in prostate cancer PDX models

We next tested Acetalax *in vivo* using two patient-derived xenograft (PDX) prostate cancer models: LuCaP147 (castration-sensitive) and LuCaP167 (castration-resistant). In both models, treatment with Acetalax significantly suppressed tumor growth with the strongest effect at 300 mg/kg. Importantly, body weight was not significantly affected,

indicating tolerability (Figure 6A-B). Immunohistochemistry (IHC) analysis confirmed TRPM4 immunoreactivity in tumor tissues. Representative images of H&E and TRPM4 staining are shown in Figure 6C. These results demonstrate that Acetalax is efficacious against both hormone-sensitive and resistant prostate tumors *in vivo* and that TRPM4 expression is maintained in these contexts.

TRPM4 is upregulated in prostate tumors but not associated with disease stage, Gleason score, or patient survival

Lastly, we examined TRPM4 expression in clinical specimens. TMA analysis revealed that TRPM4 protein expression is significantly higher in prostate adenocarcinoma than in benign prostatic hyperplasia (BPH, Figure 7A–D). Across 63 adenocarcinoma samples, 84% of cores displayed ≥85% TRPM4-positive cells, whereas only 27% of hyperplasia samples exceeded this threshold. Representative images demonstrated strong epithelial TRPM4 staining in tumor regions and weaker, focal staining in hyperplastic glands (Figure 7B–C).

To determine whether TRPM4 expression varies with tumor progression, we compared TRPM4-positive cell percentages across pathological stage and Gleason grade. TRPM4 levels were similar between stage II versus stage III–IV tumors and between Gleason score 6–7 versus 8–10 tumors, with no significant shift in the proportion of samples exceeding the ≥85% positivity threshold (Figure 7E–F). Consistent with the TMA findings, TCGA analysis showed significantly higher TRPM4 transcript levels in prostate tumors than in normal prostate tissues (Figure 7G). However, TRPM4 transcript abundance did not differ across pathological stage or Gleason score (Figure 7H–I), further indicating that TRPM4 upregulation is a marker of prostate malignancy rather than tumor aggressiveness. These findings in primary prostate cancer are complemented by analyses of metastatic mCRPC datasets, which demonstrate context-dependent TRPM4 expression across AR-driven and neuroendocrine-like tumor states.

Together, these findings demonstrate that TRPM4 is consistently upregulated in prostate cancer but does not correlate with disease progression or survival, supporting its role as a targetable biomarker of tumor identity and Acetalax sensitivity rather than a prognostic indicator.

Discussion

This study extends the previously reported anti-tumor effect on triple-negative breast cancer (TNBC) by Acetalax, an ion transport inhibitor repurposed for use as an anticancer agent with TRPM4 as a predictive biomarker for response (19,20). Acetalax activity in conjunction with TRPM4 membrane expression on tumor cells was also found in both hormone sensitive and insensitive prostate cancer, providing additional evidence of TRPM4 as a functional mediator of Acetalax sensitivity, resistance, and morphological response in different tumor models. Using an integrative approach combining *in vitro* mechanistic studies, transcriptomic profiling, and *in vivo* PDX validation in correlation between TRPM4 expression and tumor regression, we demonstrate that TRPM4 is both a predictive biomarker and a mechanistic determinant of Acetalax efficacy in prostate cancer. We propose that Acetalax acts as a TRPM4

agonists trapping the TRPM4 sodium channel in an open configuration leading to cellular swelling and oncosis.

The high levels of TRPM4 transcript in human prostate cancer tissues make Acetalax of interest as a prospective treatment for prostate cancer. We find that TRPM4 expression segregates prostate cancer cell lines into Acetalax-sensitive and -resistant subtypes. High TRPM4 expression correlates with rapid oncosis-like morphological changes, including cell swelling and blebbing, and with potent growth inhibition. Conversely, we found that TRPM4-low cells lack both morphological changes and drug sensitivity. These observations mirror prior reports in TNBC (20), underscoring TRPM4 as a generalizable determinant of Acetalax response across tumor types. Our knockdown experiments further support a functional role of TRPM4 in determining Acetalax responsiveness in prostate cancer cells. The biological relevance of these models is supported by multi-omic similarity analyses showing that PC3, LNCaP, and 22Rv1 more closely resemble patient prostate tumors than DU145, reinforcing the TRPM4-associated distinction between sensitive and resistant cell states (Supplemental Figure 4).

Our data reveal that Acetalax induces the rapid degradation of TRPM4 through the ubiquitin–proteasome system, as demonstrated by proteasome inhibition experiments. Consistently, chronic Acetalax exposure selected resistant clones with loss of TRPM4 expression, thereby establishing TRPM4 as a target of Acetalax. These results highlight TRPM4 not only as a biomarker of sensitivity but also as a vulnerable node whose absence defines therapeutic escape.

RNA-seq uncovered transcriptomic remodeling associated with TRPM4 loss. CE clones showed activation of pathways related to membrane remodeling, metabolic reprogramming, and MAPK signaling, while exhibiting repression of DNA repair and tumor suppressor programs. The TRPM4 correlation network further suggests that TRPM4 orchestrates a shift toward pro-tumorigenic signaling while suppressing protective anti-tumor pathways. These findings position TRPM4 in a hub integrating ion channel activity with oncogenic reprogramming and provide a mechanistic explanation for TRPM4's role in both sensitivity and resistance to Acetalax. In prostate cancer PDX models, Acetalax significantly suppressed tumor growth in both castration-sensitive (LuCaP147) and castration-resistant (LuCaP167) settings without affecting body weight. Although Acetalax significantly suppresses tumor growth, tumors continue to grow over time in the castration-resistant LuCaP167 model, suggesting incomplete tumor control during prolonged treatment. The efficacy observed in animal models is likely due to prodrug activation and favorable pharmacokinetics. Immunohistochemistry confirmed TRPM4 expression in PDX tumors, aligning with our *in vitro* results and supporting TRPM4 as a predictive biomarker in clinically relevant contexts. The ability of Acetalax to suppress growth in castration-resistant tumors is of particular significance, as these represent the most aggressive and treatment-refractory disease states.

Analyses of tissue microarrays and TCGA datasets revealed that TRPM4 expression is markedly upregulated in prostate cancer compared to benign tissues and other tumor types (Figure 1), yet largely unchanged across tumor stages or Gleason grades. These results suggest that TRPM4 upregulation is an early and consistent event in prostate

cancer progression, positioning TRPM4 as a broadly applicable biomarker and potential target of Acetalax independent of disease stage or grade. Analyses of metastatic mCRPC datasets further suggest that TRPM4 expression is more closely associated with AR-driven lineage features and inversely associated with neuroendocrine differentiation. These findings indicate that while TRPM4 expression is broadly elevated in primary prostate cancer, its lineage association becomes more pronounced in advanced disease states. Although direct protein-level assessment in late-stage mCRPC specimens was not performed in this study, transcriptomic analyses of metastatic cohorts indicate that TRPM4 expression varies across AR-driven and neuroendocrine-like prostate cancer subtypes, supporting its potential relevance across diverse mCRPC lineages. Importantly, while TRPM4 does not appear to predict prognosis, it robustly predicts Acetalax response, thereby fulfilling a critical unmet need for response-predictive biomarkers in prostate cancer.

Together these findings provide a rationale for the clinical development of Acetalax as a novel therapeutic option for TRPM4-expressing prostate cancers, including castration-resistant prostate cancer (CRPC). Future studies will need to evaluate Acetalax in clinical trials, explore combination strategies to prevent or overcome resistance (e.g., targeting TRPM4 degradation pathways), and extend analyses to other TRPM4-high malignancies.

In summary, our study identifies TRPM4 as a key target of Acetalax sensitivity and resistance in prostate cancer, validated by mechanistic, transcriptomic, and in vivo PDX models. These findings not only advance our understanding of TRPM4 biology but also support the repurposing of Acetalax as a targeted therapy for treatment-refractory prostate cancers.

Conclusion

TRPM4 is a central determinant of Acetalax sensitivity in prostate cancer and Acetalax suppresses tumor growth in both castration-sensitive and -resistant prostate cancer PDX models. Its expression stratifies responsive from resistant tumors and governs oncosis-like morphological responses. Loss of TRPM4 defines acquired resistance, accompanied by transcriptomic remodeling associated with tumor-promoting programs. These findings establish TRPM4 as both a predictive biomarker and a mechanistic driver of Acetalax activity, providing a rationale for repurposing Acetalax as a therapeutic option for the treatment of refractory prostate cancer.

Authors' Disclosures

No disclosures.

Authors' Contributions

Design: Y.H-K, W.C.R, N.T, Y.P, N.R.
Experiments: Y.H-K, D.T, S.K., A.L., N.Y.
Materials: Y. H-K, S.K., N.R.
Manuscript: Y. H-K, W.C.R, N.T, Y.P
Supervisor: Y.P, W.C.R, N.T

Acknowledgments

We would like to thank Madeline Wong for RNA sequencing measurements and Makito Mizunuma and Yoshihito Yokoyama for helpful discussions and advice.

This research was supported by the Intramural Research Program of the National Institutes of Health (NIH), Center for Cancer Research, National Cancer Institute (Z01 BC 006150). Additional support was provided by the Stephenson Cancer Center through internal resources and P30 CA225520 (NT).

Disclaimer

The contributions of the NIH author(s) were made as part of their official duties as NIH federal employees, are in compliance with agency policy requirements, and are considered Works of the United States Government. However, the findings and conclusions presented in this paper are those of the author(s) and do not necessarily reflect the views of the NIH or the U.S. Department of Health and Human Services.

References

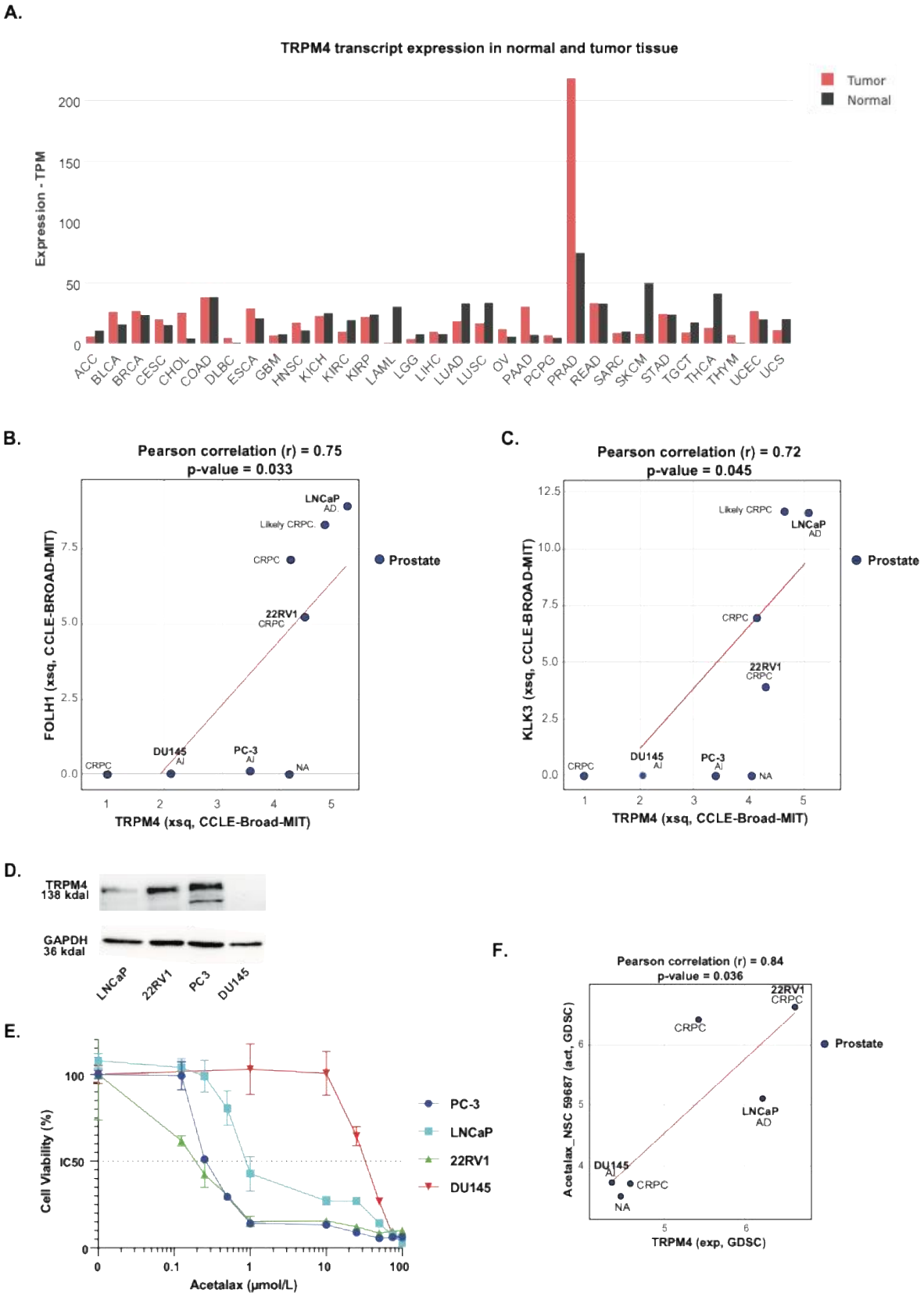
1. Torre LA, Bray F, Siegel RL, Ferlay J, Lortet-Tieulent J, Jemal A. Global cancer statistics, 2012. CA Cancer J Clin **2015**;65(2):87-108 doi 10.3322/caac.21262.
2. Tsai AK, Kagalwalla S, Langer J, Le-Kumar T, Le-Kumar V, Antonarakis ES. Pembrolizumab for metastatic castration-resistant prostate cancer: trials and tribulations. Expert Opin Biol Ther **2024**;24(1-2):51-62 doi 10.1080/14712598.2024.2311750.
3. Ferraldeschi R, Welti J, Luo J, Attard G, de Bono JS. Targeting the androgen receptor pathway in castration-resistant prostate cancer: progresses and prospects. Oncogene **2015**;34(14):1745-57 doi 10.1038/onc.2014.115.
4. Fizazi K, Tran N, Fein L, Matsubara N, Rodriguez-Antolin A, Alekseev BY*, et al.* Abiraterone acetate plus prednisone in patients with newly diagnosed high-risk metastatic castration-sensitive prostate cancer (LATITUDE): final overall survival analysis of a randomised, double-blind, phase 3 trial. Lancet Oncol **2019**;20(5):686-700 doi 10.1016/S1470-2045(19)30082-8.
5. de Bono J, Mateo J, Fizazi K, Saad F, Shore N, Sandhu S*, et al.* Olaparib for Metastatic Castration-Resistant Prostate Cancer. N Engl J Med **2020**;382(22):2091-102 doi 10.1056/NEJMoa1911440.
6. Fizazi K, Piulats JM, Reaume MN, Ostler P, McDermott R, Gingerich JR*, et al.* Rucaparib or Physician's Choice in Metastatic Prostate Cancer. N Engl J Med **2023**;388(8):719-32 doi 10.1056/NEJMoa2214676.
7. Chi KN, Rathkopf D, Smith MR, Efstathiou E, Attard G, Olmos D*, et al.* Niraparib and Abiraterone Acetate for Metastatic Castration-Resistant Prostate Cancer. J Clin Oncol **2023**;41(18):3339-51 doi 10.1200/JCO.22.01649.
8. Egevad L, Micoli C, Delahunt B, Samaratunga H, Garmo H, Stattin P*, et al.* Gleason scores provide more accurate prognostic information than grade groups. Pathology **2025**;57(3):293-6 doi 10.1016/j.pathol.2024.12.633.
9. Campa J, Mar-Barrutia G, Extramiana J, Arrospide A, Mar J. Advanced prostate cancer survival in Spain according to the Gleason score, age and stage. Actas Urol Esp **2016**;40(8):499-506 doi 10.1016/j.acuro.2016.03.008.
10. Steele CB, Li J, Huang B, Weir HK. Prostate cancer survival in the United States by race and stage (2001-2009): Findings from the CONCORD-2 study. Cancer **2017**;123 Suppl 24(Suppl 24):5160-77 doi 10.1002/cncr.31026.
11. Sagredo AI, Sagredo EA, Pola V, Echeverria C, Andaur R, Michea L*, et al.* TRPM4 channel is involved in regulating epithelial to mesenchymal transition, migration, and invasion of prostate cancer cell lines. J Cell Physiol **2019**;234(3):2037-50 doi 10.1002/jcp.27371.
12. Holzmann C, Kappel S, Kilch T, Jochum MM, Urban SK, Jung V*, et al.* Transient receptor potential melastatin 4 channel contributes to migration of androgen-insensitive prostate cancer cells. Oncotarget **2015**;6(39):41783-93 doi 10.18632/oncotarget.6157.
13. Ashida S, Nakagawa H, Katagiri T, Furihata M, Iiizumi M, Anazawa Y*, et al.* Molecular features of the transition from prostatic intraepithelial neoplasia (PIN) to prostate cancer: genome-wide gene-expression profiles of prostate cancers and PINs. Cancer Res **2004**;64(17):5963-72 doi 10.1158/0008-5472.CAN-04-0020.

14. Berg KD, Soldini D, Jung M, Dietrich D, Stephan C, Jung K*, et al.* TRPM4 protein expression in prostate cancer: a novel tissue biomarker associated with risk of biochemical recurrence following radical prostatectomy. Virchows Arch **2016**;468(3):345-55 doi 10.1007/s00428-015-1880-y.
15. Schinke EN, Bii V, Nalla A, Rae DT, Tedrick L, Meadows GG*, et al.* A novel approach to identify driver genes involved in androgen-independent prostate cancer. Mol Cancer **2014**;13:120 doi 10.1186/1476-4598-13-120.
16. Sagredo AI, Sagredo EA, Cappelli C, Baez P, Andaur RE, Blanco C*, et al.* TRPM4 regulates Akt/GSK3-beta activity and enhances beta-catenin signaling and cell proliferation in prostate cancer cells. Mol Oncol **2018**;12(2):151-65 doi 10.1002/1878-0261.12100.
17. Morrison BL, Mullendore ME, Stockwin LH, Borgel S, Hollingshead MG, Newton DL. Oxyphenisatin acetate (NSC 59687) triggers a cell starvation response leading to autophagy, mitochondrial dysfunction, and autocrine TNFalpha-mediated apoptosis. Cancer Med **2013**;2(5):687-700 doi 10.1002/cam4.107.
18. Rajapakse VN, Luna A, Yamade M, Loman L, Varma S, Sunshine M*, et al.* CellMinerCDB for Integrative Cross-Database Genomics and Pharmacogenomics Analyses of Cancer Cell Lines. iScience **2018**;10:247-64 doi 10.1016/j.isci.2018.11.029.
19. Mizunuma M, Redon CE, Saha LK, Tran AD, Dhall A, Sebastian R*, et al.* Acetalax (Oxyphenisatin Acetate, NSC 59687) and Bisacodyl Cause Oncosis in Triple-Negative Breast Cancer Cell Lines by Poisoning the Ion Exchange Membrane Protein TRPM4. Cancer Res Commun **2024**;4(8):2101-11 doi 10.1158/2767-9764.CRC-24-0093.
20. Reinhold WC, Marangoni E, Elloumi F, Montagne R, Varma S, Wang Y*, et al.* Acetalax and Bisacodyl for the Treatment of Triple-Negative Breast Cancer: A Combined Molecular and Preclinical Study. Cancer Res Commun **2025**;5(2):375-88 doi 10.1158/2767-9764.CRC-24-0435.
21. Luna A, Elloumi F, Varma S, Wang Y, Rajapakse VN, Aladjem MI*, et al.* CellMiner Cross-Database (CellMinerCDB) version 1.2: Exploration of patient-derived cancer cell line pharmacogenomics. Nucleic Acids Res **2021**;49(D1):D1083-D93 doi 10.1093/nar/gkaa968.
22. Ohgane K, Yoshioka H. Quantification of gel bands by an ImageJ macro, Band/Peak Quantification Tool v1. Protocolsio **2019** doi 10.17504/protocols.io.7vghn3w.
23. Amin MB, Greene FL, Edge SB, Compton CC, Gershenwald JE, Brookland RK*, et al.* The Eighth Edition AJCC Cancer Staging Manual: Continuing to build a bridge from a population-based to a more "personalized" approach to cancer staging. CA Cancer J Clin **2017**;67(2):93-9 doi 10.3322/caac.21388.
24. Sinha R, Luna A, Schultz N, Sander C. A pan-cancer survey of cell line tumor similarity by feature-weighted molecular profiles. Cell Rep Methods **2021**;1(2):100039 doi 10.1016/j.crmeth.2021.100039.
25. Sevilla S, Sovacool K, Kuhn S, Tandon M, Koparda V. Rna sEquencing aNalysis pipElinE (v2.7.1). zenodo **2025**(v2.7.1).

26. Dobin A, Davis CA, Schlesinger F, Drenkow J, Zaleski C, Jha S*, et al.* STAR: ultrafast universal RNA-seq aligner. Bioinformatics **2013**;29(1):15-21 doi 10.1093/bioinformatics/bts635.
27. Liberzon A, Birger C, Thorvaldsdottir H, Ghandi M, Mesirov JP, Tamayo P. The Molecular Signatures Database (MSigDB) hallmark gene set collection. Cell Syst **2015**;1(6):417-25 doi 10.1016/j.cels.2015.12.004.
28. Kohn KW, Zeeberg BM, Reinhold WC, Pommier Y. Gene expression correlations in human cancer cell lines define molecular interaction networks for epithelial phenotype. PLoS One **2014**;9(6):e99269 doi 10.1371/journal.pone.0099269.
29. Arner E, Daub CO, Vitting-Seerup K, Andersson R, Lilje B, Drablos F*, et al.* Transcribed enhancers lead waves of coordinated transcription in transitioning mammalian cells. Science **2015**;347(6225):1010-4 doi 10.1126/science.1259418.
30. Roper N, Velez MJ, Chiappori A, Kim YS, Wei JS, Sindiri S*, et al.* Notch signaling and efficacy of PD-1/PD-L1 blockade in relapsed small cell lung cancer. Nat Commun **2021**;12(1):3880 doi 10.1038/s41467-021-24164-y.

Figure Legends

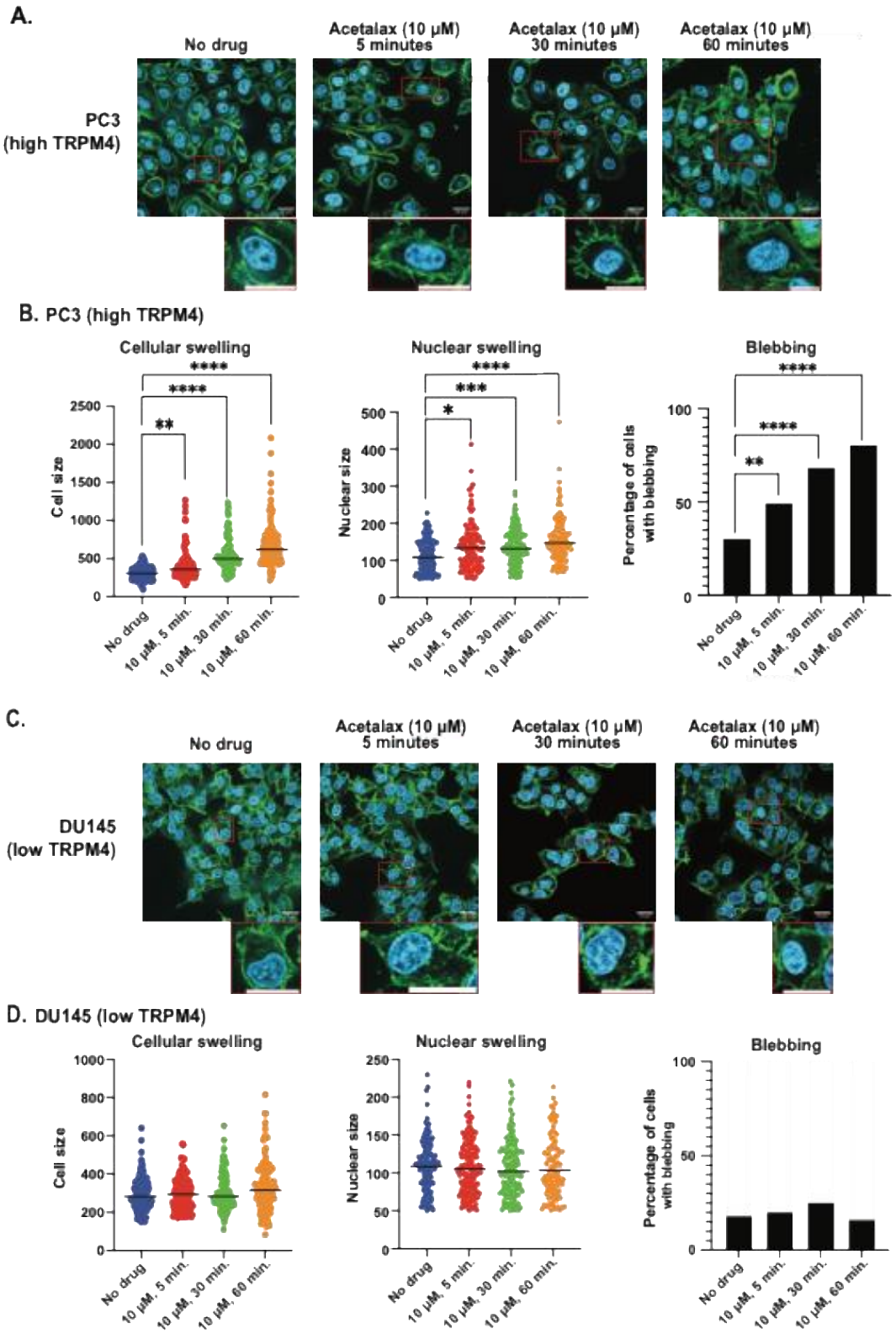
Figure 1


A.
TRPM4 transcript expression in normal and tumor tissue
Tumor
Normal
Expression - TPM
ACC BLCA BRCA CESC CHOL COAD DLBC ESCA GBM HNSC KICH KIRC KIRP LAML LGG LIHC LUAD LUSC OV PAAD PCPG PRAD READ SARC SKCM STAD TGCT THCA THYM UCEC UCS
B.
Pearson correlation (r) = 0.75
p-value = 0.033
FOLH1 (xsq, CCLE-BROAD-MIT)
TRPM4 (xsq, CCLE-Broad-MIT)
Prostate
LNCaP AD.
Likely CRPC.
CRPC
22RV1 CRPC
DU145 AI
PC-3 AI
NA
C.
Pearson correlation (r) = 0.72
p-value = 0.045
KLK3 (xsq, CCLE-BROAD-MIT)
TRPM4 (xsq, CCLE-Broad-MIT)
Prostate
Likely CRPC
LNCaP AD
CRPC
22RV1 CRPC
DU145 AI
PC-3 AI
NA
D.
TRPM4 138 kdal
GAPDH 36 kdal
LNCaP
22RV1
PC3
DU145
E.
Cell Viability (%)
IC50
Acetalax (µmol/L)
PC-3
LNCaP
22RV1
DU145
F.
Pearson correlation (r) = 0.84
p-value = 0.036
Acetalax_NSC 59687 (act, GDSC)
TRPM4 (exp, GDSC)
Prostate
22RV1 CRPC
CRPC
LNCaP AD
DU145 AI
CRPC
NA

1

Figure 1: TRPM4 transcript expression in normal and cancerous tissue and prostate cell lines, and Acetalax activity in cancerous prostate cell lines.
A. Bar plot of the gene transcript expression profile across all Gene Expression Profiling Interactive Analysis (GEPIA2) paired tumor and normal samples. The x-axis is the tissues and y-axis the transcript level in each transcript per million (TPM). ACC is adrenocortical carcinoma, BLCA is bladder urothelial cancer, BRCA is breast carcinoma, CESC is cervical squamous cell carcinoma and endocervical, CHOL is cholangiocarcinoma, COAD is colon adenocarcinoma, DLBC is Lymphoid Neoplasm Diffuse Large B-cell Lymphoma, LAML is Acute Myeloid Leukemia, LGG is brain lower grade glioma, ESDA is esophageal carcinoma, GBM is Glioblastoma multiforme, HNSC is head and neck squamous cell carcinoma, KICH is kidney chromophobe, KIRC is kidney renal clear cell carcinoma, KIRP is kidney renal clear cell, LIHC is liver hepatocellular carcinoma, LUAD is lung adenocarcinoma, LUSC is lung squamous cell carcinoma, OV is ovarian serous cystadenocarcinoma, PAAD is pancreatic adenocarcinoma, PCPG is pheochromocytoma and paraganglioma, PRAD is prostate adenocarcinoma, READ is rectal adenocarcinoma, SARC is sarcoma, SKCM is skin cutaneous melanoma, STAD is stomach, TGCT is testicular germ cell tumors, THCA is thyroid carcinoma, THYM is thymoma, UCEC is uterine corpus endometrial cancer, and UCS is uterine carcinosarcoma.
B. Scatter plot of *TRPM4* (x-axis) versus *FOLH1* (PSMA, y-axis) transcription expression for prostate cancer (8 cell lines). Both are CCLE-BROAD-MIT RNA-seq. The red line is the regression line. Each circle is a cell line.
C. Same as panel B with *KLK3* (PSA, y-axis) transcription expression for prostate cancer (8 cell lines). Visualization for **B** and **C** are done using CellMinerCDB.
D. Western blot showing higher TRPM4 expression in Acetalax-sensitive cell lines (PC3, LNCaP, 22Rv1) compared with DU145.
E. Cell viability assays for four prostate cell lines measured at 72 hours using ATPlite 1-step. Experiments were performed in triplicate. Bars represent 1 standard deviation.
F. Correlation between *TRPM4* transcript levels and Acetalax sensitivity (IC50) across prostate cancer cell lines in the GDSC dataset, showing a strong positive association consistent with panel D.
Abbreviations: AD, androgen-dependent; AI, androgen-independent; CRPC, castration-resistant prostate cancer.

Figure 2


A.
No drug
Acetalax (10 µM) 5 minutes
Acetalax (10 µM) 30 minutes
Acetalax (10 µM) 60 minutes
PC3 (high TRPM4)
B. PC3 (high TRPM4)
Cellular swelling
Nuclear swelling
Blebbing
Cell size
Nuclear size
Percentage of cells with blebbing
No drug
10 µM, 5 min.
10 µM, 30 min.
10 µM, 60 min.
C.
DU145 (low TRPM4)
D. DU145 (low TRPM4)

1

Figure 2: Morphological changes caused by Acetalax in prostate cell lines PC3 and DU145.

A. Representative microscopy images of PC3 cells treated with Acetalax (10 µM for 5, 30 or 60 min) and stained in blue with DAPI (binds DNA) and green with phalloidin (stains actin). Scale bars indicate 20 µm.

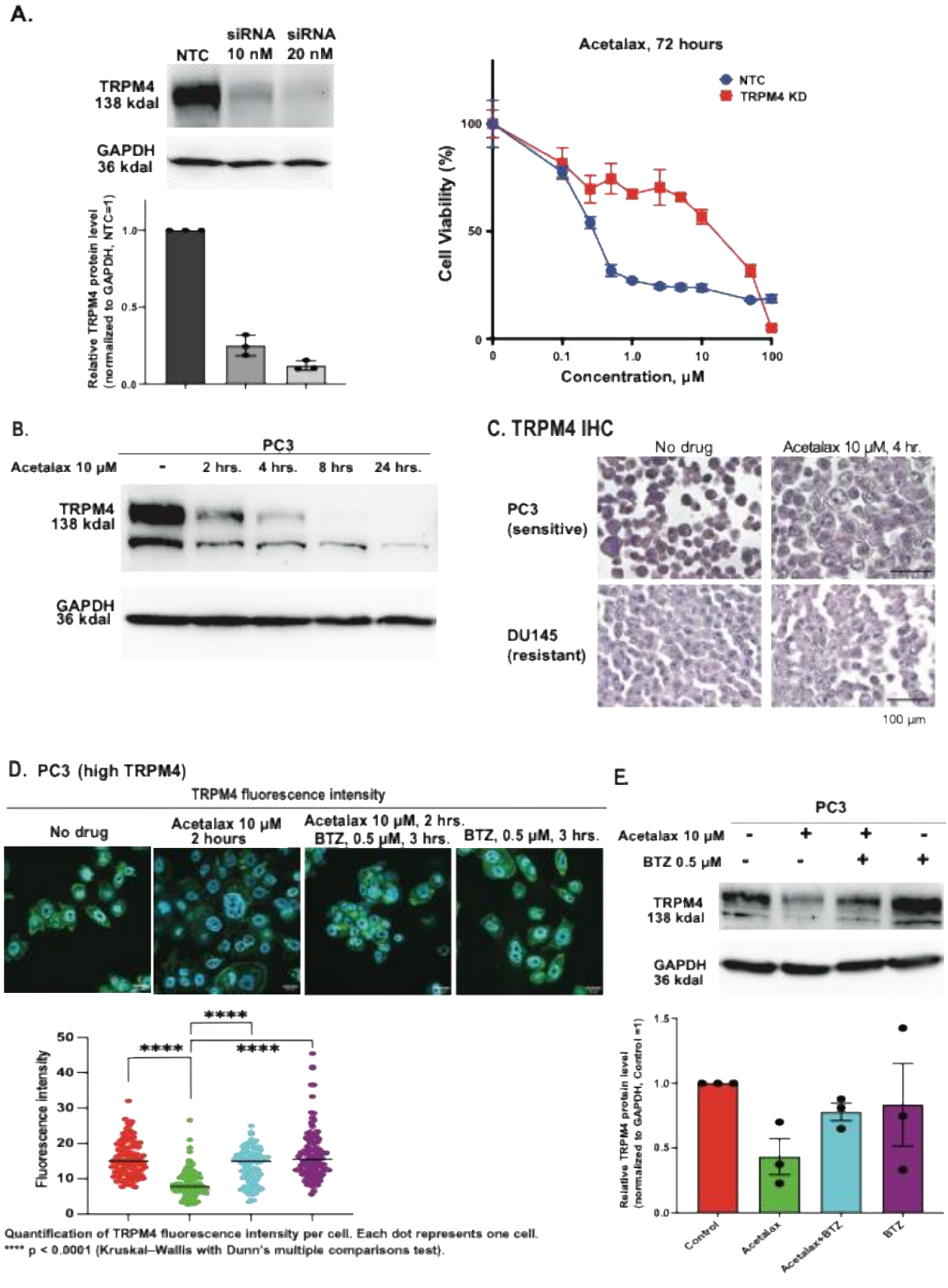
B. The PC3 scatter plots quantitate cell and nuclear size upon treatment with 10 µM Acetalax for the indicated times. The bar plot quantitates the observed blebbing. Statistical significance is indicated: * for $p<0.05$, ** for $p<0.01$, *** for $p<0.005$, and **** for $p<0.0001$ (by Kruskal-Wallis test, the Dunn's multiple comparisons test), calculated in PRISM 10.

C. Representative microscopy images of Acetalax-resistant DU145 cells treated with Acetalax (10 µM for 5, 30 or 60 min) and stained in blue with DAPI (binds DNA) and green with phalloidin (stains actin). Scale bars indicate 20 µm.

D. The DU145 scatter plots quantitate cell and nuclear size upon treatments for 5, 30 and 60 minutes with 10 µM Acetalax. The bar plot quantitates the observed blebbing. There is no significant change for any of the three plots. For both B and D, the number of cells counted for cell size and blebbing is 100. For nuclear size, the cells counted was between 100 and 139 per group. The horizontal lines within the scatter plots indicate medians and the circles individual cells.

High-magnification views of the boxed regions are shown below each panel to visualize Acetalax-induced cellular swelling and blebbing. Note the different scales for the expanded images.

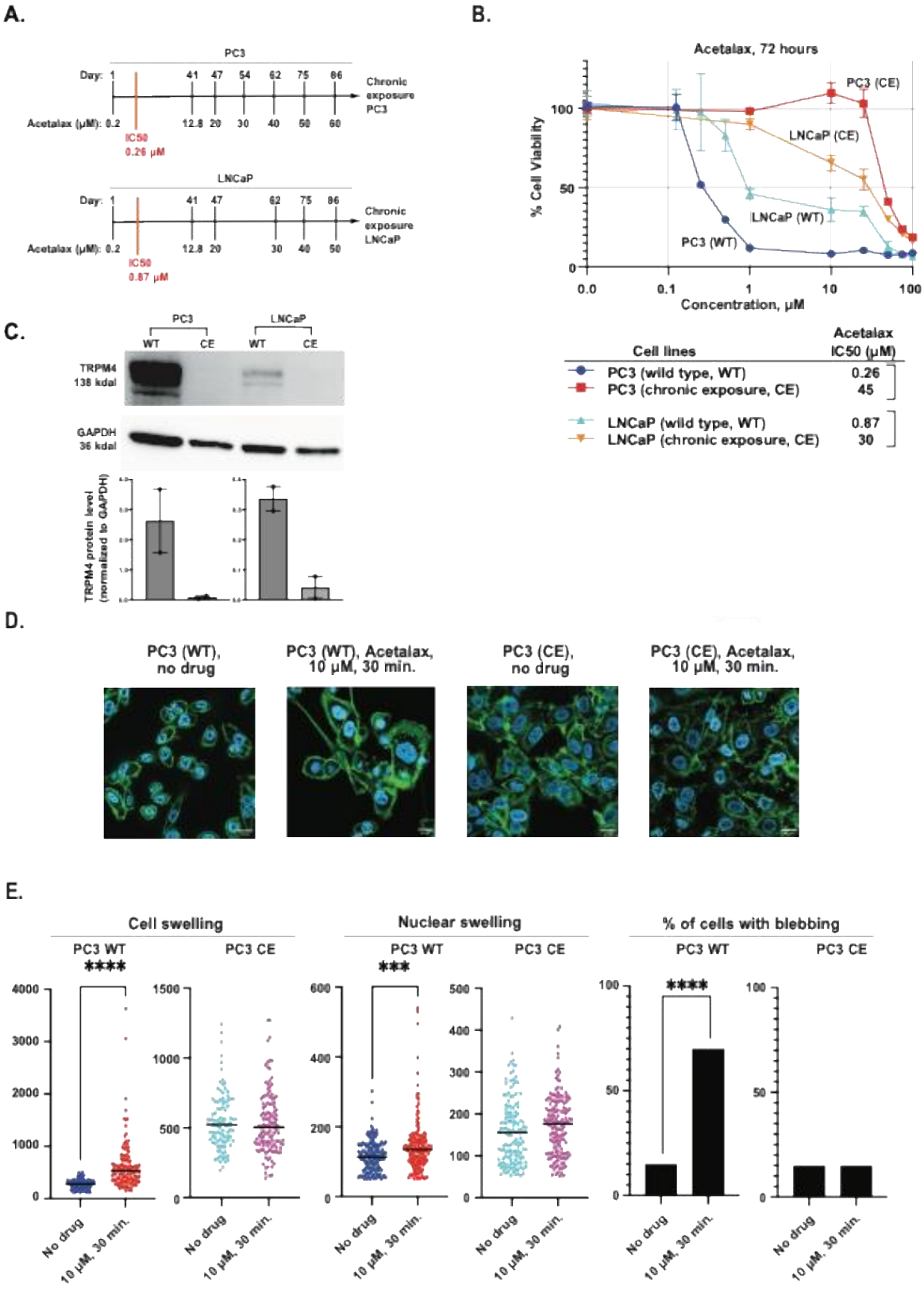
Figure 3


A.
NTC
siRNA 10 nM
siRNA 20 nM
TRPM4 138 kdal
GAPDH 36 kdal
Relative TRPM4 protein level (normalized to GAPDH, NTC=1)
Acetalax, 72 hours
NTC
TRPM4 KD
Cell Viability (%)
Concentration, µM
B.
PC3
Acetalax 10 µM
2 hrs.
4 hrs.
8 hrs
24 hrs.
TRPM4 138 kdal
GAPDH 36 kdal
C. TRPM4 IHC
No drug
Acetalax 10 µM, 4 hr.
PC3 (sensitive)
DU145 (resistant)
100 µm
D. PC3 (high TRPM4)
TRPM4 fluorescence intensity
No drug
Acetalax 10 µM 2 hours
Acetalax 10 µM, 2 hrs. BTZ, 0.5 µM, 3 hrs.
BTZ, 0.5 µM, 3 hrs.
Fluorescence intensity
****
Quantification of TRPM4 fluorescence intensity per cell. Each dot represents one cell.
**** p < 0.0001 (Kruskal–Wallis with Dunn's multiple comparisons test).
E
PC3
Acetalax 10 µM
BTZ 0.5 µM
TRPM4 138 kdal
GAPDH 36 kdal
Relative TRPM4 protein level (normalized to GAPDH, Control =1)
Control
Acetalax
Acetalax+BTZ
BTZ

1

Figure 3: TRPM4 protein expression and degradation in response to Acetalax.
A. TRPM4 knockdown reduces sensitivity to Acetalax in PC3 cells. Western blot analysis showing TRPM4 protein levels following siRNA-mediated knockdown, with GAPDH as loading control. Quantification of TRPM4 protein levels normalized to GAPDH is shown below. Drug response curves (DRC) demonstrate reduced sensitivity to Acetalax in TRPM4 knockdown (KD) cells compared with negative control (NTC).
B. Time-dependent reduction of TRPM4 protein following Acetalax treatment. PC3 cells were treated with Acetalax (10 μM) for the indicated times.
C. Immunohistochemical analysis of TRPM4 expression in prostate cancer cell lines. PC3 (Acetalax-sensitive) and DU145 (Acetalax-resistant) cells were treated with or without Acetalax (10 μM for 4 hours) and stained using a TRPM4 mouse monoclonal antibody (1:200 dilution). Scale bar, 100 μm.
D. Immunofluorescence Microscopy of TRPM4 degradation induced by Acetalax and its blockage by bortezomib. Representative images of Acetalax-sensitive PC3 cell lines treated without or with Acetalax (10 μM for 2 hours) and/or the proteosome inhibitor bortezomib (BTZ, 0.5 μM, 3 hours) and stained for TRPM4 protein and DNA (blue with DAPI). Scale bars (on the bottom right of images) indicate 20 microns (μm). Quantification of TRPM4 fluorescence intensity is shown below. Statistical significance between the indicated groups was determined by Kruskal–Wallis test followed by Dunn's multiple-comparisons test (****, $p < 0.0001$).
E. Western blot of TRPM4 levels in PC3 cells treated with Acetalax and/or bortezomib (BTZ) as indicated. In panels A, B and F, GAPDH is used as loading control. Quantification of TRPM4 levels normalized to GAPDH is shown below.

Figure 4


A.
PC3
Day: 1 41 47 54 62 75 86
Chronic exposure PC3
Acetalax (μM): 0.2 12.8 20 30 40 50 60
IC50 0.26 μM
LNCaP
Day: 1 41 47 62 75 86
Chronic exposure LNCaP
Acetalax (μM): 0.2 12.8 20 30 40 50
IC50 0.87 μM
B.
Acetalax, 72 hours
% Cell Viability
Concentration, μM
PC3 (CE)
LNCaP (CE)
LNCaP (WT)
PC3 (WT)
Cell lines
Acetalax IC50 (μM)
PC3 (wild type, WT) 0.26
PC3 (chronic exposure, CE) 45
LNCaP (wild type, WT) 0.87
LNCaP (chronic exposure, CE) 30
C.
PC3
LNCaP
WT
CE
TRPM4 138 kdal
GAPDH 36 kdal
TRPM4 protein level (normalized to GAPDH)
D.
PC3 (WT), no drug
PC3 (WT), Acetalax, 10 μM, 30 min.
PC3 (CE), no drug
PC3 (CE), Acetalax, 10 μM, 30 min.
E.
Cell swelling
Nuclear swelling
% of cells with blebbing
PC3 WT
PC3 CE
****
***
No drug
10 μM, 30 min.

1

Figure 4: Characterization of Acetalax-resistant cells obtained by chronic drug exposure.

A. Flow chart of development of Acetalax-resistant PC3 and LNCaP chronic exposure (CE) cell lines. WT is wild type. IC50 is inhibitory concentration 50%.

B. Acetalax cell viability assay in wild type and CE cells. Acetalax treatments at the indicated concentrations (x-axis) were for 72 hours. Cell viability (y-axis) was determined using ATPlite 2. Experiments were performed in triplicate. The IC50s of the wild type and CE versions of the cell lines are compared (bottom table).

C. Western blot of TRPM4 expression in PC3 and LNCaP WT and Acetalax-resistant CE cells. GAPDH is used as loading control. TRPM4 band intensity was quantified and normalized to GAPDH from two independent experiments. Values represent relative TRPM4 protein levels (TRPM4/GAPDH).

D. Representative microscopy images of wild type PC3 cells and their resistant (CE) derivative with and without Acetalax treatment. Cells were stained in blue with DAPI (binds DNA) and green with phalloidin (stains actin). Acetalax treatments were at 10 µM for 30 minutes. Scale bars indicate 20 µm.

E. PC3 wild type versus chronic exposure comparisons of cell swelling (left), nuclear swelling (center) and cell blebbing (right) of the panel D results. Each cell is indicated by a circle for the cell and nuclear swelling.

Figure 5

A.

TRPM4 transcription expression (RNAseq)

Gene \ Sample	PC3 Parental	PC3 Acetalax, 10 μM, 4hr	PC3 Chronic exposure	LNCaP Parental	LNCaP Acetalax, 10 μM, 4hr	LNCaP Chronic exposure
TRPM4	4.95	5.50	3.60	6.11	6.02	2.84

B.

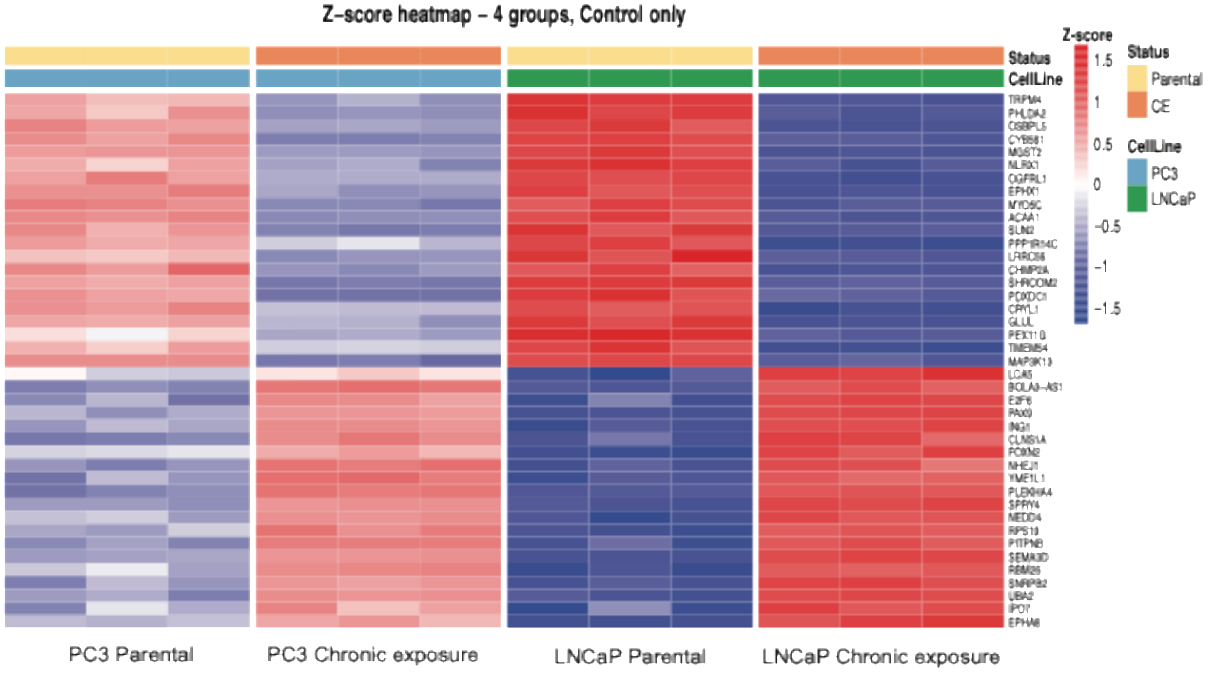
Oncogenic pathways upregulated during chronic exposure in both PC3 and LNCaP

NES (PC3)	NES (LNCaP)	Common Pathways
2.36	2.08	HALLMARK_E2F_TARGETS
2.23	2.10	HALLMARK_G2M_CHECKPOINT
2.11	2.24	HALLMARK_MYC_TARGETS_V1
1.71	1.38	HALLMARK_DNA_REPAIR
1.60	1.77	KOHN_EMT_MESENCHYMAL
1.49	1.24	HALLMARK_SPERMATOGENESIS
1.45	1.45	HALLMARK_WNT_BETA_CATENIN_SIGNALING
1.44	1.83	HALLMARK_MYC_TARGETS_V2
1.29	1.33	HALLMARK_MITOTIC_SPINDLE
1.19	1.05	HALLMARK_MTORC1_SIGNALING
1.12	1.58	HALLMARK_ANGIOGENESIS

Oncogenic pathways downregulated during chronic exposure in both PC3 and LNCaP

NES (PC3)	NES (LNCaP)	Common Pathways
-2.00	-1.01	HALLMARK_TNFA_SIGNALING_VIA_NFKB
-1.99	-1.89	KOHN_EMT_EPITHELIAL
-1.97	-1.63	HALLMARK_ESTROGEN_RESPONSE_EARLY
-1.69	-0.93	HALLMARK_IL6_JAK_STAT3_SIGNALING
-1.67	-1.41	EMT_58
-1.67	-1.44	EMT_37
-1.64	-1.42	HALLMARK_P53_PATHWAY
-1.55	-1.39	HALLMARK_ESTROGEN_RESPONSE_LATE
-1.51	-1.24	HALLMARK_HYPOXIA
-1.48	-1.84	HALLMARK_ANDROGEN_RESPONSE
-1.34	-1.26	HALLMARK_XENOBIOTIC_METABOLISM

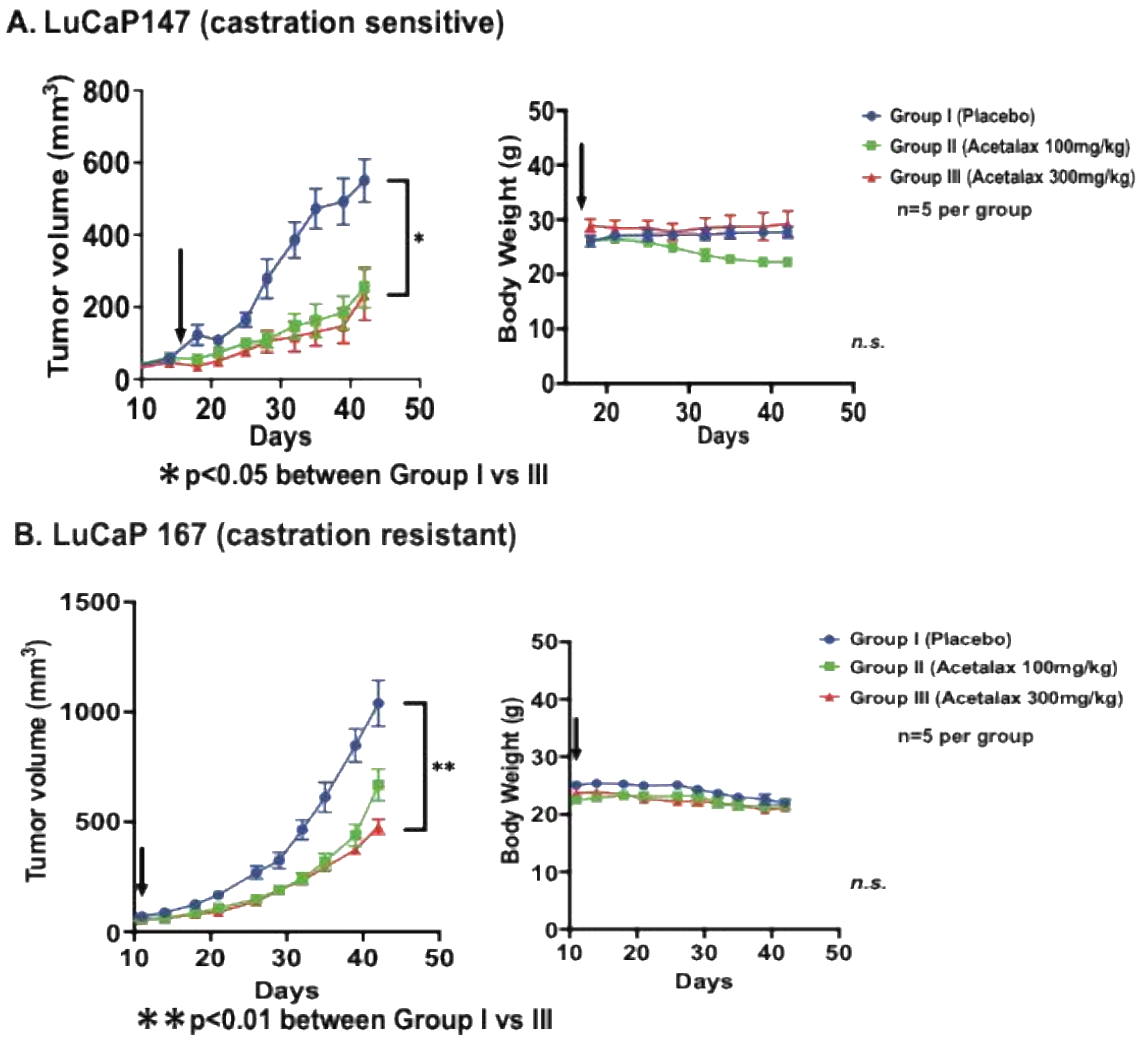
C.



1

Figure 5. Transcriptomic changes associated with TRPM4 loss following chronic Acetalax exposure.
A. TRPM4 transcript levels in parental and chronic exposure (CE) cells, with or without short-term Acetalax treatment.
B. Gene set enrichment analysis (GSEA) comparing CE versus parental PC3 and LNCaP cells. Pathways upregulated during chronic exposure (left) include E2F targets, MYC targets, metabolic and membrane-remodeling programs, and MAPK signaling. Downregulated pathways (right) include DNA repair, p53 signaling, androgen response, and inflammatory and stress-response pathways.
C. Heatmap of the top TRPM4-correlated genes, derived by calculating TRPM4–gene correlations across all RNA-seq samples (PC3 and LNCaP parental and CE, with and without short-term exposure). The top 20 positively and negatively correlated genes are displayed. Expression levels are shown for control conditions only, comparing parental versus chronic-exposure (CE) cells in PC3 and LNCaP. Positively correlated genes are enriched for membrane-associated and metabolic functions, whereas negatively correlated genes include DNA repair genes, tumor suppressors, and regulators of epithelial differentiation. Within-group variation represents biological triplicates, indicating reproducible yet biologically meaningful variability across samples.

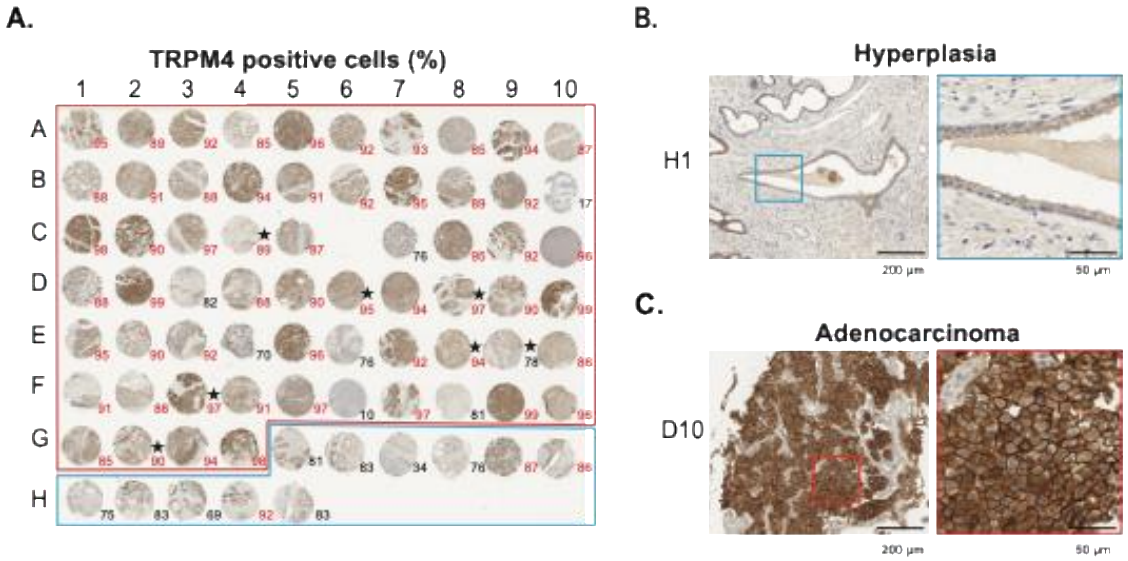
Figure 6

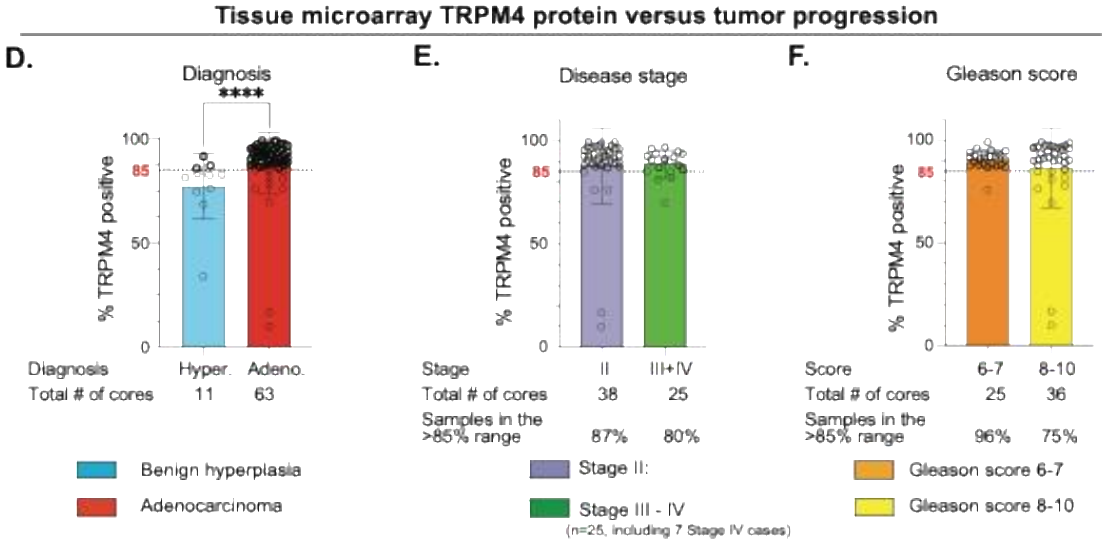

A. LuCaP147 (castration sensitive)
Tumor volume (mm3)
Days
*
Body Weight (g)
Days
n.s.
Group I (Placebo)
Group II (Acetalax 100mg/kg)
Group III (Acetalax 300mg/kg)
n=5 per group
* p<0.05 between Group I vs III
B. LuCaP 167 (castration resistant)
Tumor volume (mm3)
Days
**
Body Weight (g)
Days
n.s.
Group I (Placebo)
Group II (Acetalax 100mg/kg)
Group III (Acetalax 300mg/kg)
n=5 per group
** p<0.01 between Group I vs III
C. PDX IHC
No drug
100 mg/kg
300 mg/kg
H&E
TRPM4
50μm

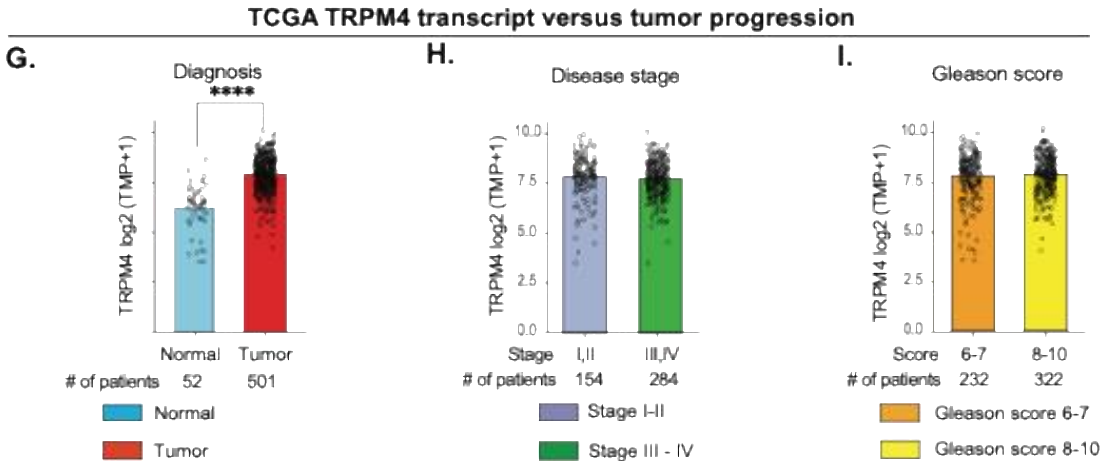
1

Figure 6. Acetalax suppresses tumor growth in prostate cancer PDX models.
A. LuCaP147 (castration-sensitive) PDX: tumor growth curves and body weight changes. Acetalax at either 100 or 300 mg/kg statistically significantly reduced tumor growth vs. placebo. Body weight did not change significantly. Data are mean ± SEM (n = 5 mice per group). * $p<0.05$.
B. LuCaP167 (castration-resistant) PDX: tumor growth curves and body weight changes, showing similar significant tumor suppression without significant body weight loss. Data are mean ± SEM (n = 5 mice per group). ** $p<0.01$.
C. Representative H&E and TRPM4 IHC images of PDX tumors (Placebo vs Acetalax 300 mg/kg).
Note: Prostate PDX staining shown in this figure was performed manually; antibody concentration was optimized to prevent non-specific background, resulting in lower staining intensity compared with automated staining shown in Figure 7.

Figure 7


A.
TRPM4 positive cells (%)
1 2 3 4 5 6 7 8 9 10
A
B
C
D
E
F
G
H
B.
Hyperplasia
H1
200 µm
50 µm
C.
Adenocarcinoma
D10
200 µm
50 µm


Tissue microarray TRPM4 protein versus tumor progression
D.
Diagnosis
****
% TRPM4 positive
100
85
50
0
Diagnosis Hyper. Adeno.
Total # of cores 11 63
Benign hyperplasia
Adenocarcinoma
E.
Disease stage
% TRPM4 positive
Stage II III+IV
Total # of cores 38 25
Samples in the >85% range 87% 80%
Stage II:
Stage III - IV
(n=25, including 7 Stage IV cases)
F.
Gleason score
% TRPM4 positive
Score 6-7 8-10
Total # of cores 25 36
Samples in the >85% range 96% 75%
Gleason score 6-7
Gleason score 8-10


TCGA TRPM4 transcript versus tumor progression
G.
Diagnosis
****
TRPM4 log2 (TMP+1)
Normal Tumor
# of patients 52 501
Normal
Tumor
H.
Disease stage
TRPM4 log2 (TMP+1)
10.0
7.5
5.0
2.5
0.0
Stage I,II III,IV
# of patients 154 284
Stage I-II
Stage III - IV
I.
Gleason score
TRPM4 log2 (TMP+1)
Score 6-7 8-10
# of patients 232 322
Gleason score 6-7
Gleason score 8-10

1

Figure 7: TRPM4 expression in prostate tissue microarray and TCGA patient samples.

A. Tissue microarray cores stained for TRPM4 protein for 74 patients. The rows are labeled A through H and the columns 1 through 10. The adenocarcinomas are within the red box, and the hyperplasia within the blue box.

B. TMA magnified images of hyperplasia core H1 (from panel A). The blue box in the left panel (10x) identifies the area of the sample shown in the enlarged right panel (40X).

C. TMA magnified images of adenocarcinoma core D10 (from panel A). The red box in the left panel (10x) identifies the area of the sample shown in the enlarged right panel (40x).

D. TMA box/scatter plot of the percent TRPM4 positive cells distribution for hyperplasias (hyper.) as compared to adenocarcinomas (adeno.). The stars indicate a statistically significant change with **** indicating $p<0.0001$.

E. TMA box/scatter plot of the percent TRPM4 positive cells distribution for adenocarcinomas in Stage II as compared to Stage III and IV adenocarcinomas. Stage indicates amount of and spread of cancer, with lower Stage indicating less spread and higher more.

F. TMA box/scatter plot of the percent TRPM4 positive cells distribution for adenocarcinomas in Gleason score 6-7 as compared to Gleason score 8-10. Gleason grade indicates the amount of microscopy-based difference from normal prostate tissue, with lower values indicating less and higher more. For panels D-F the horizontal dotted line demarks 85%. Each circle is a patient core. The error bars indicate standard deviation.

G. The Cancer Genome Atlas (TCGA) box/scatter plot of the TRPM4 transcript level distribution for normal as compared to tumor tissue. The star indicates a statistically significant change (unpaired t test with Welch's correction done in PRISM. $p<0.0001$.

H. TCGA box/scatter plot of the of the TRPM4 transcript level distribution for stage I and II as compared to stage III and IV tumors.

I. TCGA box/scatter plot of the of the TRPM4 transcript level distribution for Gleason score 6 and 7 as compared to Gleason score 8 to 10 tumors.

Figure 1

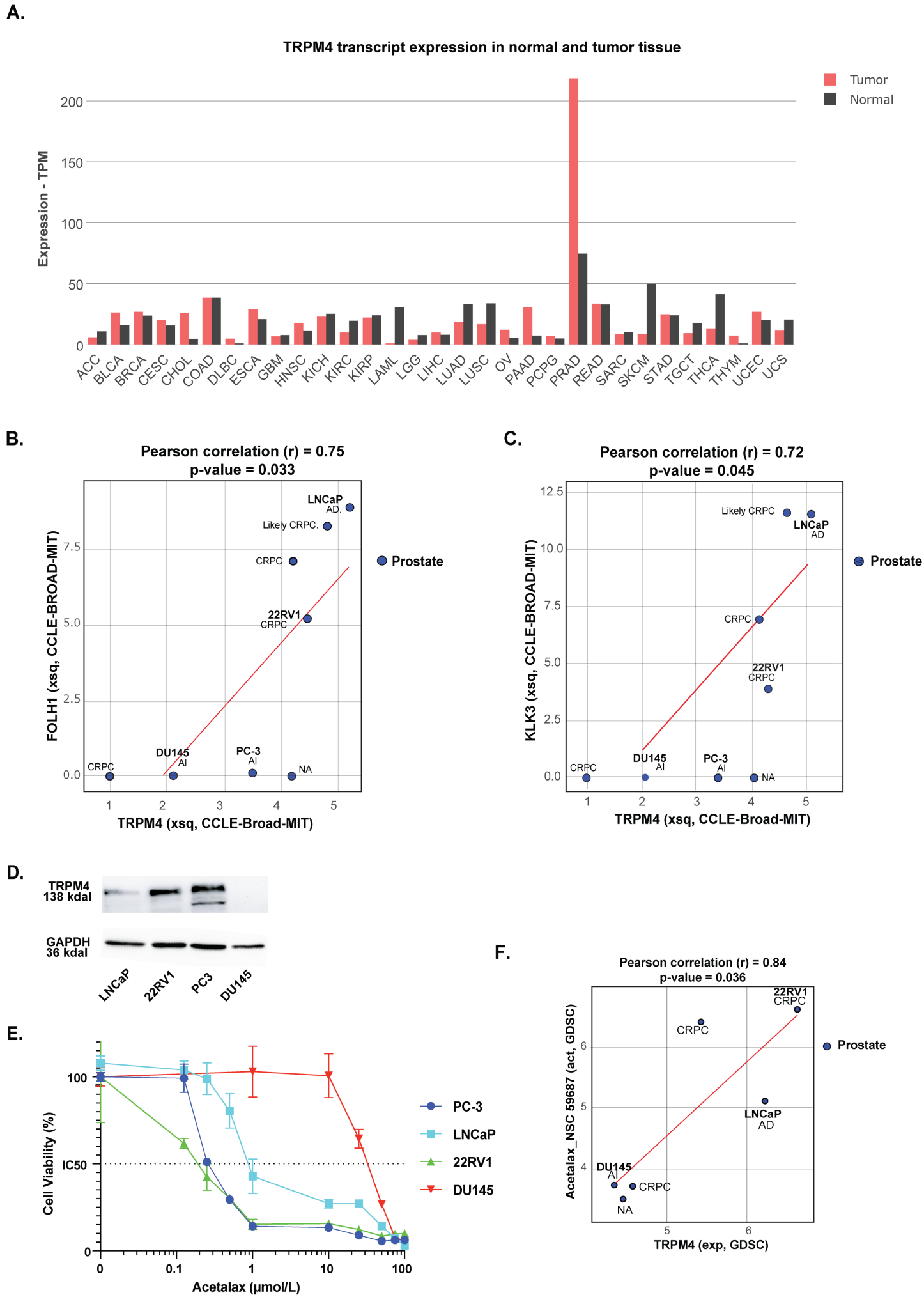

A.
TRPM4 transcript expression in normal and tumor tissue
Tumor
Normal
Expression - TPM
200
150
100
50
0
ACC BLCA BRCA CESC CHOL COAD DLBC ESCA GBM HNSC KICH KIRC KIRP LAML LGG LIHC LUAD LUSC OV PAAD PCPG PRAD READ SARC SKCM STAD TGCT THCA THYM UCEC UCS
B.
Pearson correlation (r) = 0.75
p-value = 0.033
LNCaP AD.
Likely CRPC.
CRPC
22RV1 CRPC
DU145 AI
PC-3 AI
NA
CRPC
Prostate
FOLH1 (xsq, CCLE-BROAD-MIT)
TRPM4 (xsq, CCLE-Broad-MIT)
C.
Pearson correlation (r) = 0.72
p-value = 0.045
Likely CRPC
LNCaP AD
CRPC
22RV1 CRPC
DU145 AI
PC-3 AI
NA
CRPC
Prostate
KLK3 (xsq, CCLE-BROAD-MIT)
TRPM4 (xsq, CCLE-Broad-MIT)
D.
TRPM4
138 kdal
GAPDH
36 kdal
LNCaP
22RV1
PC3
DU145
E.
Cell Viability (%)
IC50
PC-3
LNCaP
22RV1
DU145
Acetalax (µmol/L)
F.
Pearson correlation (r) = 0.84
p-value = 0.036
22RV1 CRPC
CRPC
LNCaP AD
DU145 AI
CRPC
NA
Prostate
Acetalax_NSC 59687 (act, GDSC)
TRPM4 (exp, GDSC)

Figure 2

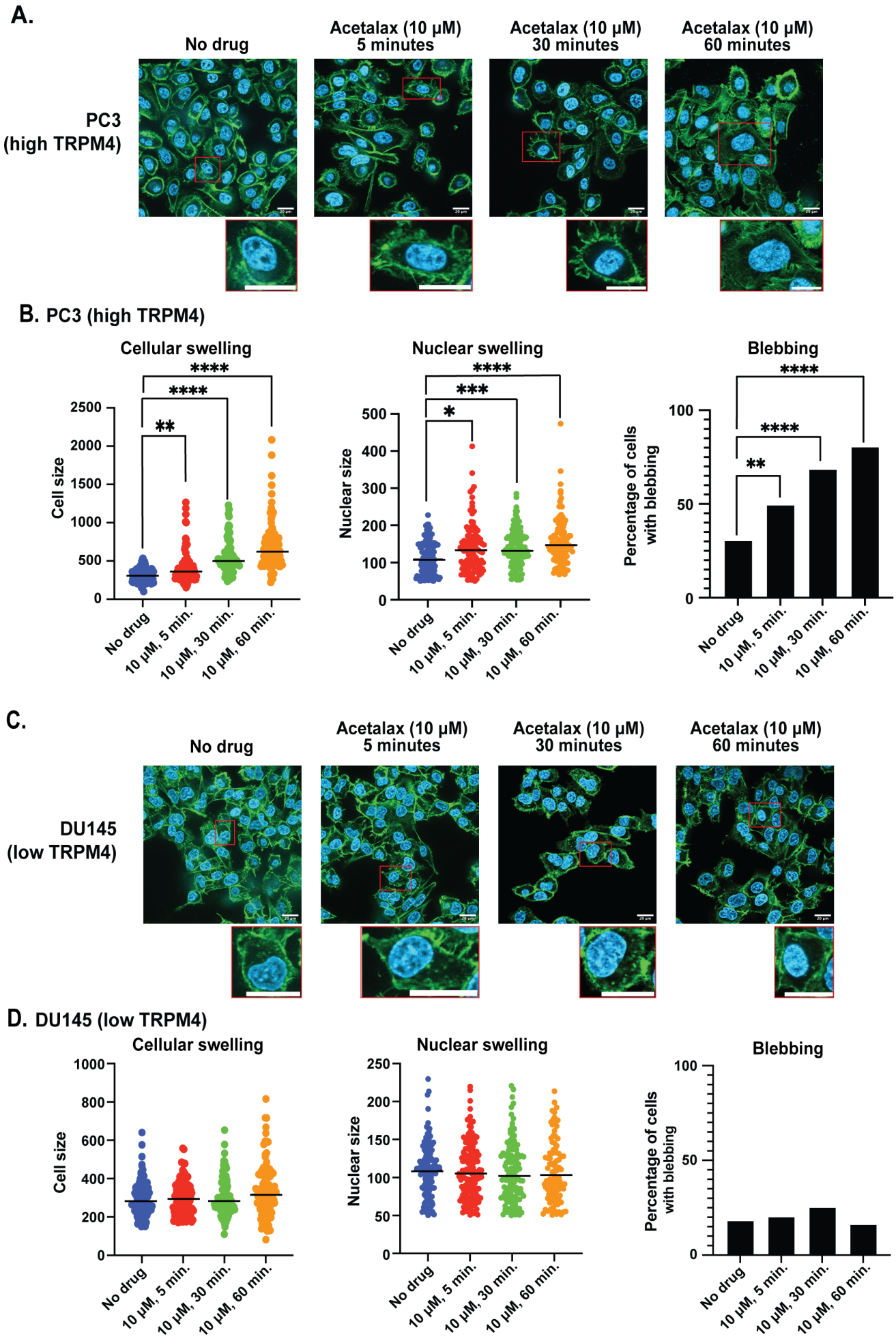
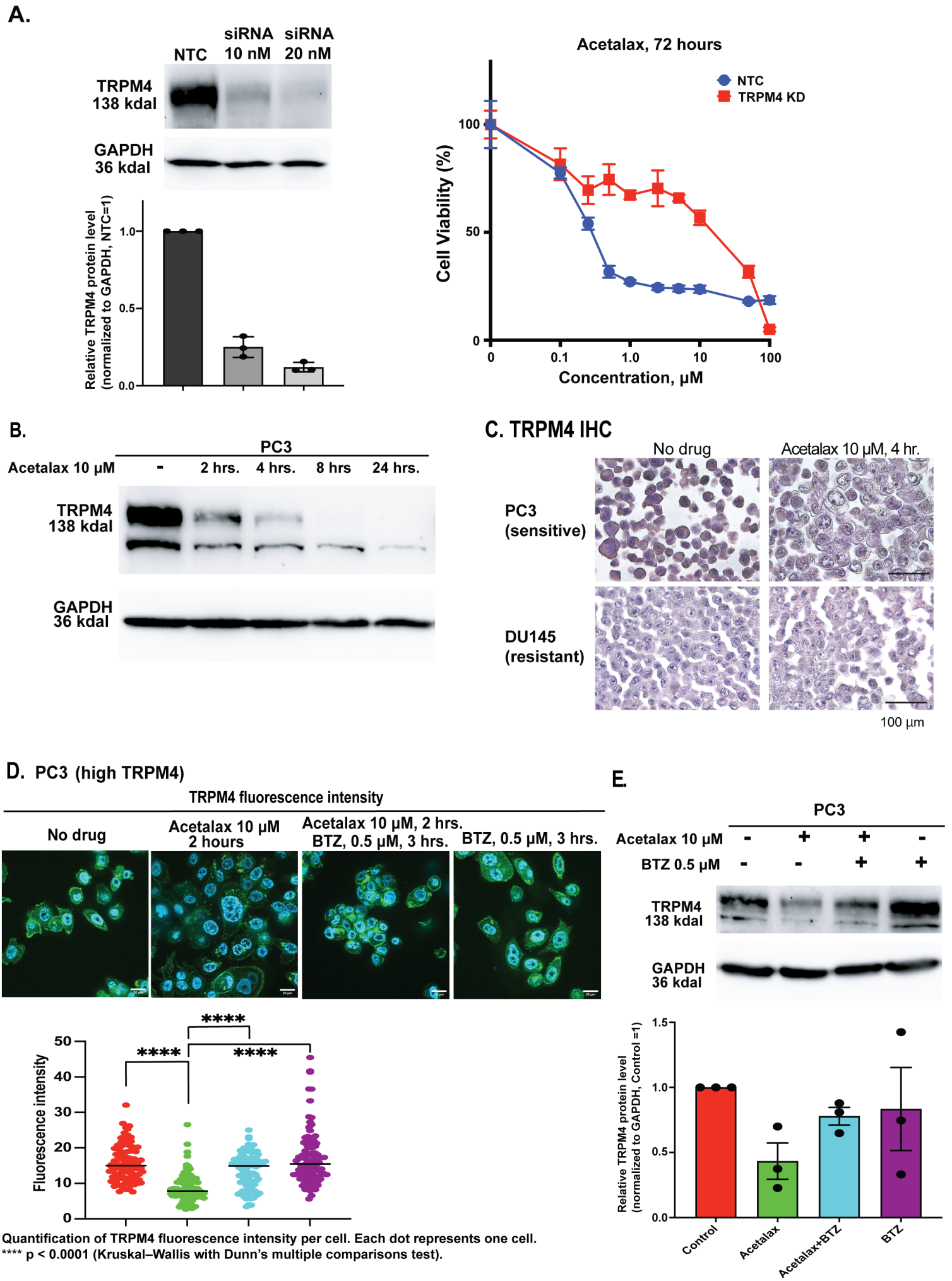

A.
No drug
Acetalax (10 µM) 5 minutes
Acetalax (10 µM) 30 minutes
Acetalax (10 µM) 60 minutes
PC3 (high TRPM4)
B. PC3 (high TRPM4)
Cellular swelling
Cell size
Nuclear swelling
Nuclear size
Blebbing
Percentage of cells with blebbing
No drug
10 µM, 5 min.
10 µM, 30 min.
10 µM, 60 min.
C.
DU145 (low TRPM4)
D. DU145 (low TRPM4)

Figure 3



Quantification of TRPM4 fluorescence intensity per cell. Each dot represents one cell.
**** $p < 0.0001$ (Kruskal–Wallis with Dunn's multiple comparisons test).

Figure 4

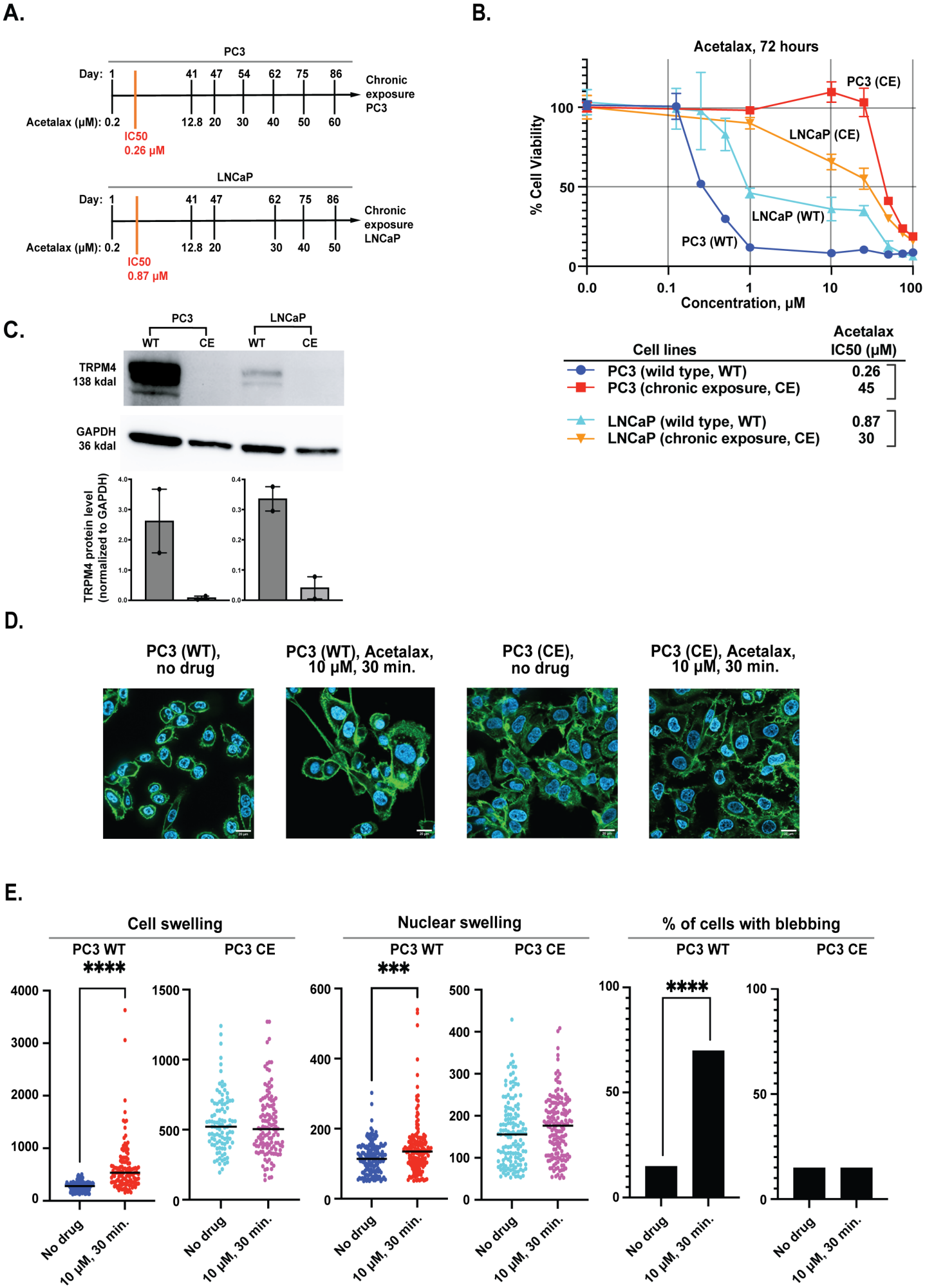

A.
PC3
Day: 1 41 47 54 62 75 86
Chronic exposure PC3
Acetalax (μM): 0.2 12.8 20 30 40 50 60
IC50 0.26 μM
LNCaP
Day: 1 41 47 62 75 86
Chronic exposure LNCaP
Acetalax (μM): 0.2 12.8 20 30 40 50
IC50 0.87 μM
B.
Acetalax, 72 hours
% Cell Viability
Concentration, μM
PC3 (CE)
LNCaP (CE)
LNCaP (WT)
PC3 (WT)
Cell lines
Acetalax IC50 (μM)
PC3 (wild type, WT) 0.26
PC3 (chronic exposure, CE) 45
LNCaP (wild type, WT) 0.87
LNCaP (chronic exposure, CE) 30
C.
PC3
LNCaP
WT
CE
TRPM4 138 kdal
GAPDH 36 kdal
TRPM4 protein level (normalized to GAPDH)
D.
PC3 (WT), no drug
PC3 (WT), Acetalax, 10 μM, 30 min.
PC3 (CE), no drug
PC3 (CE), Acetalax, 10 μM, 30 min.
E.
Cell swelling
Nuclear swelling
% of cells with blebbing
PC3 WT
PC3 CE
****
***
No drug
10 μM, 30 min.

Figure 5

A.

TRPM4 transcription expression (RNAseq)

Gene \ Sample	PC3 Parental	PC3 Acetalax, 10 μM, 4hr	PC3 Chronic exposure	LNCaP Parental	LNCaP Acetalax, 10 μM, 4hr	LNCaP Chronic exposure
TRPM4	4.95	5.50	3.60	6.11	6.02	2.84

B.

Oncogenic pathways upregulated during chronic exposure in both PC3 and LNCaP

NES (PC3)	NES (LNCaP)	Common Pathways
2.36	2.08	HALLMARK_E2F_TARGETS
2.23	2.10	HALLMARK_G2M_CHECKPOINT
2.11	2.24	HALLMARK_MYC_TARGETS_V1
1.71	1.38	HALLMARK_DNA_REPAIR
1.60	1.77	KOHN_EMT_MESENCHYMAL
1.49	1.24	HALLMARK_SPERMATOGENESIS
1.45	1.45	HALLMARK_WNT_BETA_CATENIN_SIGNALING
1.44	1.83	HALLMARK_MYC_TARGETS_V2
1.29	1.33	HALLMARK_MITOTIC_SPINDLE
1.19	1.05	HALLMARK_MTORC1_SIGNALING
1.12	1.58	HALLMARK_ANGIOGENESIS

Oncogenic pathways downregulated during chronic exposure in both PC3 and LNCaP

NES (PC3)	NES (LNCaP)	Common Pathways
-2.00	-1.01	HALLMARK_TNFA_SIGNALING_VIA_NFKB
-1.99	-1.89	KOHN_EMT_EPITHELIAL
-1.97	-1.63	HALLMARK_ESTROGEN_RESPONSE_EARLY
-1.69	-0.93	HALLMARK_IL6_JAK_STAT3_SIGNALING
-1.67	-1.41	EMT_58
-1.67	-1.44	EMT_37
-1.64	-1.42	HALLMARK_P53_PATHWAY
-1.55	-1.39	HALLMARK_ESTROGEN_RESPONSE_LATE
-1.51	-1.24	HALLMARK_HYPOXIA
-1.48	-1.84	HALLMARK_ANDROGEN_RESPONSE
-1.34	-1.26	HALLMARK_XENOBIOTIC_METABOLISM

C.

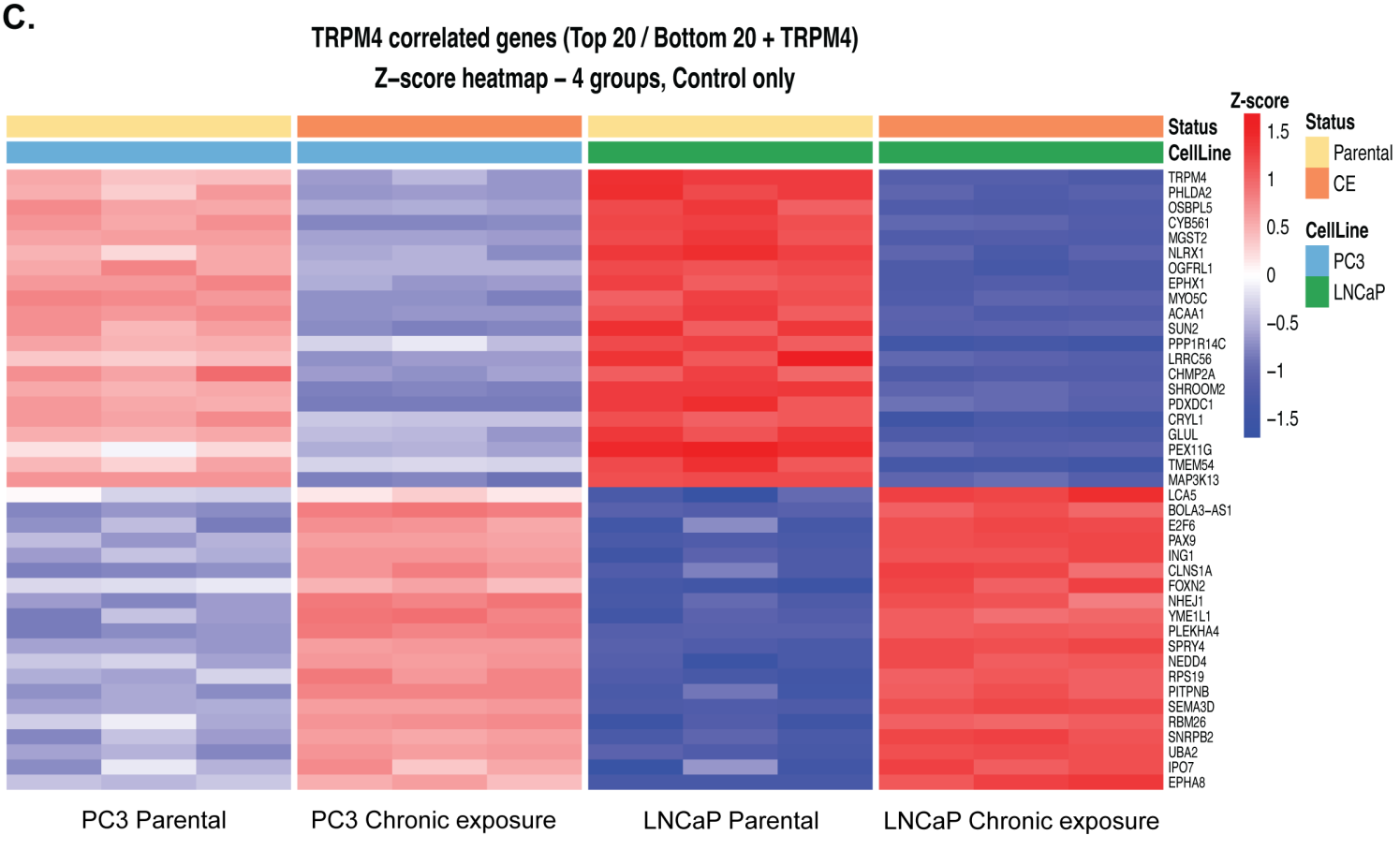
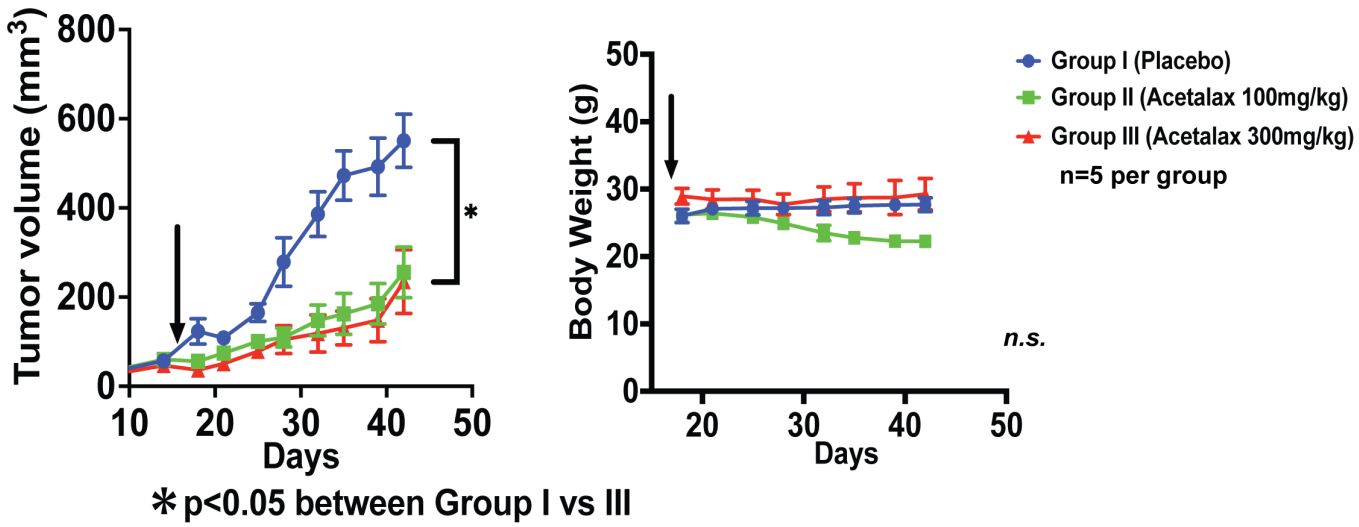


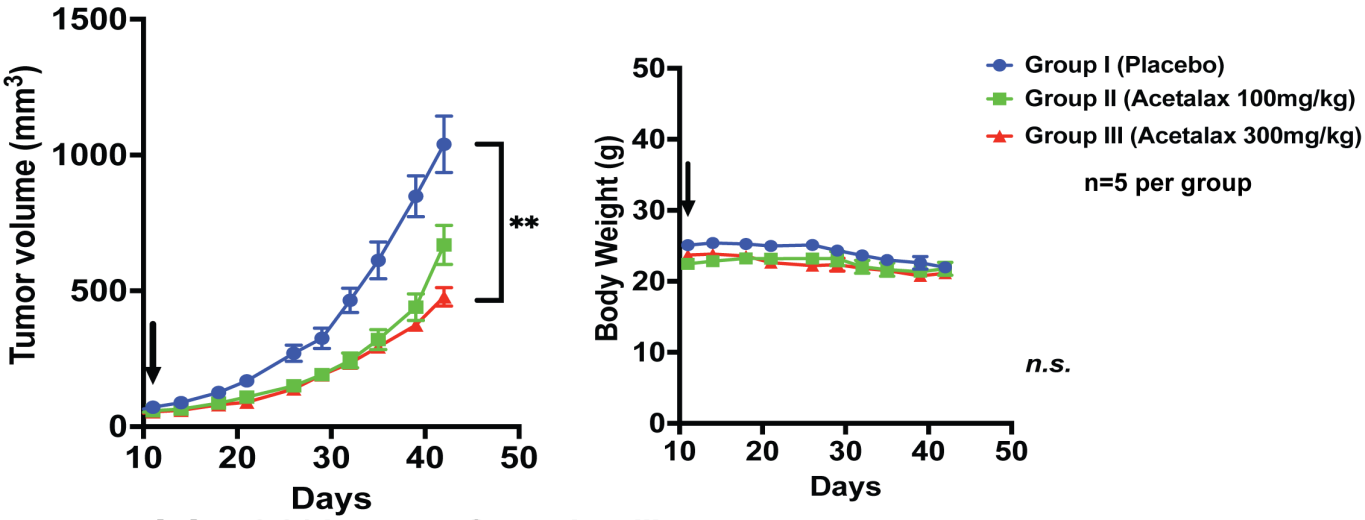
Figure 6

A. LuCaP147 (castration sensitive)



＊p<0.05 between Group I vs III

B. LuCaP 167 (castration resistant)



＊＊p<0.01 between Group I vs III

C. PDX IHC

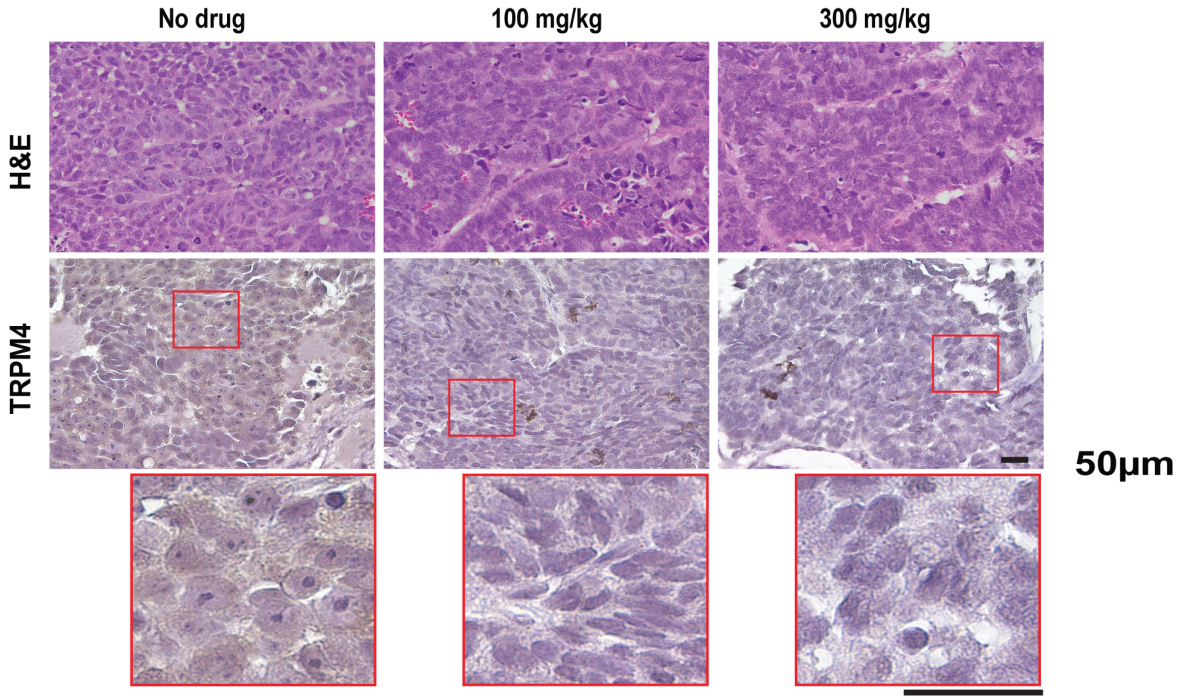
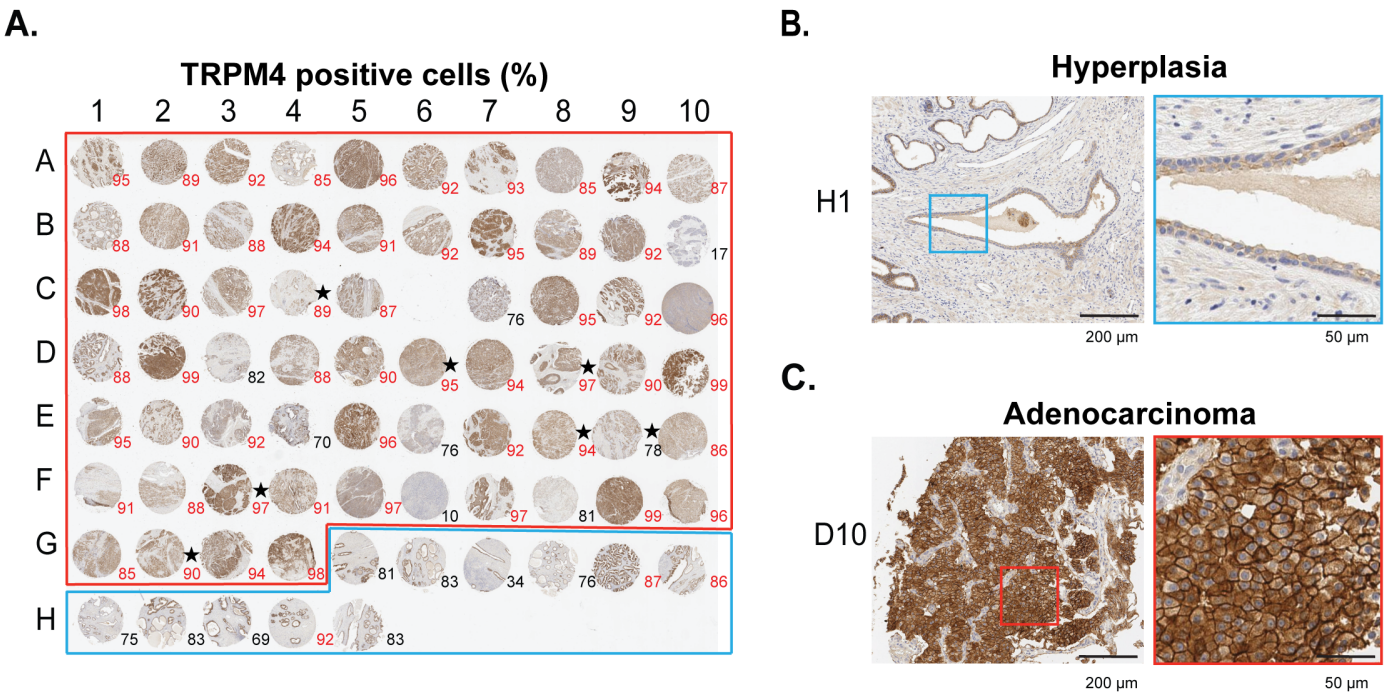
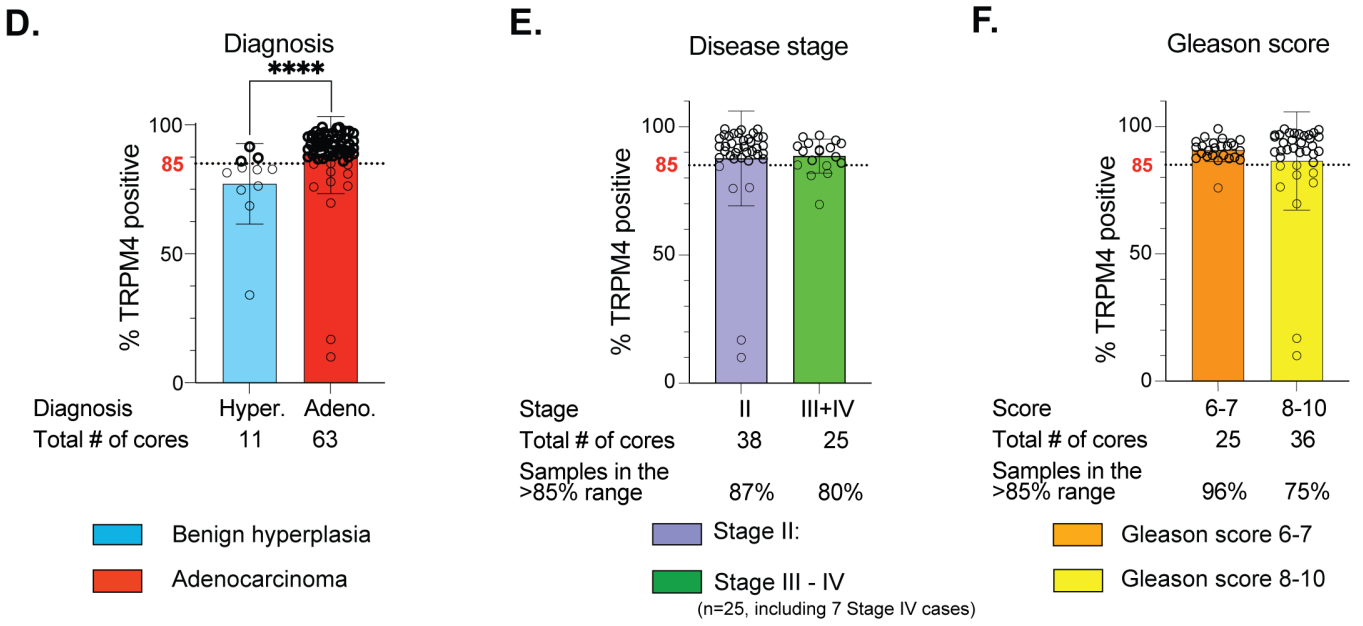


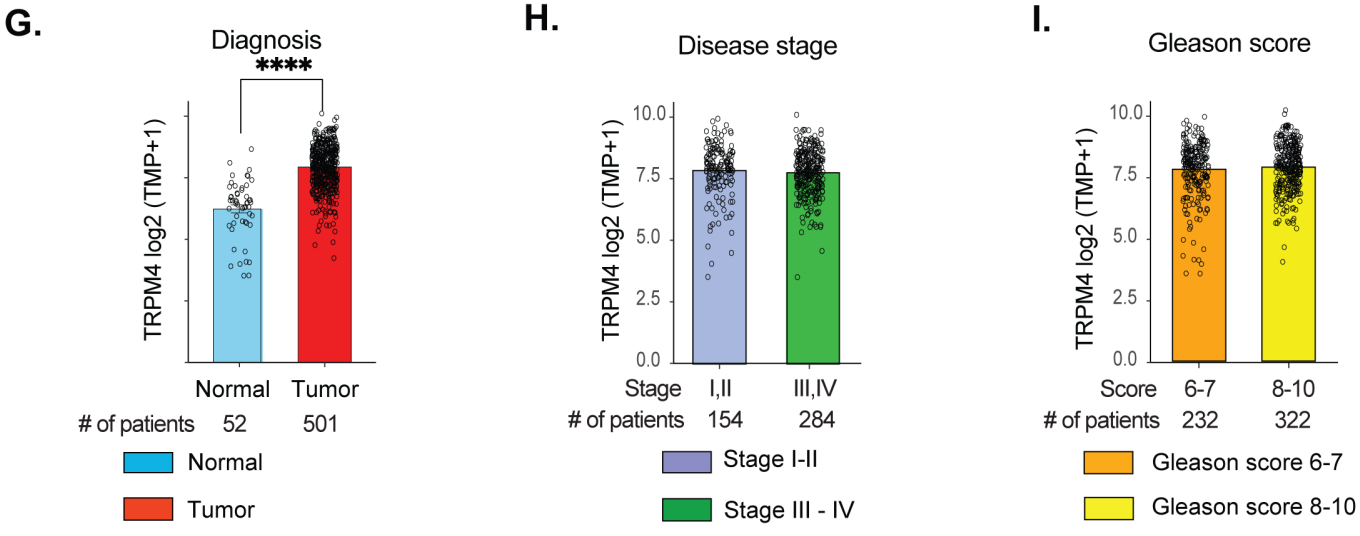
Figure 7



Tissue microarray TRPM4 protein versus tumor progression



TCGA TRPM4 transcript versus tumor progression



Parsed Citations

1. Torre LA, Bray F, Siegel RL, Ferlay J, Lortet-Tieulent J, Jemal A. Global cancer statistics, 2012. CA Cancer J Clin 2015;65(2):87-108 doi 10.3322/caac.21262.

Pubmed: Author and Title
CrossRef: Author and Title
Google Scholar: Google Scholar Search

2. Tsai AK, Kagalwalla S, Langer J, Le-Kumar T, Le-Kumar V, Antonarakis ES. Pembrolizumab for metastatic castration-resistant prostate cancer: trials and tribulations. Expert Opin Biol Ther 2024;24(1-2):51-62 doi 10.1080/14712598.2024.2311750.

Pubmed: Author and Title
CrossRef: Author and Title
Google Scholar: Google Scholar Search

3. Ferraldeschi R, Welti J, Luo J, Attard G, de Bono JS. Targeting the androgen receptor pathway in castration-resistant prostate cancer: progresses and prospects. Oncogene 2015;34(14):1745-57 doi 10.1038/onc.2014.115.

Pubmed: Author and Title
CrossRef: Author and Title
Google Scholar: Google Scholar Search

4. Fizazi K, Tran N, Fein L, Matsubara N, Rodriguez-Antolin A, Alekseev BY, et al. Abiraterone acetate plus prednisone in patients with newly diagnosed high-risk metastatic castration-sensitive prostate cancer (LATITUDE): final overall survival analysis of a randomised, double-blind, phase 3 trial. Lancet Oncol 2019;20(5):686-700 doi 10.1016/S1470-2045(19)30082-8.

Pubmed: Author and Title
CrossRef: Author and Title
Google Scholar: Google Scholar Search

5. de Bono J, Mateo J, Fizazi K, Saad F, Shore N, Sandhu S, et al. Olaparib for Metastatic Castration-Resistant Prostate Cancer. N Engl J Med 2020;382(22):2091-102 doi 10.1056/NEJMoa1911440.

Pubmed: Author and Title
CrossRef: Author and Title
Google Scholar: Google Scholar Search

6. Fizazi K, Piulats JM, Reaume MN, Ostler P, McDermott R, Gingerich JR, et al. Rucaparib or Physician's Choice in Metastatic Prostate Cancer. N Engl J Med 2023;388(8):719-32 doi 10.1056/NEJMoa2214676.

Pubmed: Author and Title
CrossRef: Author and Title
Google Scholar: Google Scholar Search

7. Chi KN, Rathkopf D, Smith MR, Efstathiou E, Attard G, Olmos D, et al. Niraparib and Abiraterone Acetate for Metastatic Castration-Resistant Prostate Cancer. J Clin Oncol 2023;41(18):3339-51 doi 10.1200/JCO.22.01649.

Pubmed: Author and Title
CrossRef: Author and Title
Google Scholar: Google Scholar Search

8. Egevad L, Micoli C, Delahunt B, Samaratunga H, Garmo H, Stattin P, et al. Gleason scores provide more accurate prognostic information than grade groups. Pathology 2025;57(3):293-6 doi 10.1016/j.pathol.2024.12.633.

Pubmed: Author and Title
CrossRef: Author and Title
Google Scholar: Google Scholar Search

9. Campa J, Mar-Barrutia G, Extramiana J, Arrospide A, Mar J. Advanced prostate cancer survival in Spain according to the Gleason score, age and stage. Actas Urol Esp 2016;40(8):499-506 doi 10.1016/j.acuro.2016.03.008.

Pubmed: Author and Title
CrossRef: Author and Title

Google Scholar: Google Scholar Search

10. Steele CB, Li J, Huang B, Weir HK. Prostate cancer survival in the United States by race and stage (2001-2009): Findings from the CONCORD-2 study. Cancer 2017;123 Suppl 24(Suppl 24):5160-77 doi 10.1002/cncr.31026.
Pubmed: Author and Title
CrossRef: Author and Title
Google Scholar: Google Scholar Search

11. Sagredo AI, Sagredo EA, Pola V, Echeverria C, Andaur R, Michea L, et al. TRPM4 channel is involved in regulating epithelial to mesenchymal transition, migration, and invasion of prostate cancer cell lines. J Cell Physiol 2019;234(3):2037-50 doi 10.1002/jcp.27371.
Pubmed: Author and Title
CrossRef: Author and Title
Google Scholar: Google Scholar Search

12. Holzmann C, Kappel S, Kilch T, Jochum MM, Urban SK, Jung V, et al. Transient receptor potential melastatin 4 channel contributes to migration of androgen-insensitive prostate cancer cells. Oncotarget 2015;6(39):41783-93 doi 10.18632/oncotarget.6157.
Pubmed: Author and Title
CrossRef: Author and Title
Google Scholar: Google Scholar Search

13. Ashida S, Nakagawa H, Katagiri T, Furihata M, Iiizumi M, Anazawa Y, et al. Molecular features of the transition from prostatic intraepithelial neoplasia (PIN) to prostate cancer: genome-wide gene-expression profiles of prostate cancers and PINs. Cancer Res 2004;64(17):5963-72 doi 10.1158/0008-5472.CAN-04-0020.
Pubmed: Author and Title
CrossRef: Author and Title
Google Scholar: Google Scholar Search

14. Berg KD, Soldini D, Jung M, Dietrich D, Stephan C, Jung K, et al. TRPM4 protein expression in prostate cancer: a novel tissue biomarker associated with risk of biochemical recurrence following radical prostatectomy. Virchows Arch 2016;468(3):345-55 doi 10.1007/s00428-015-1880-y.
Pubmed: Author and Title
CrossRef: Author and Title
Google Scholar: Google Scholar Search

15. Schinke EN, Bii V, Nalla A, Rae DT, Tedrick L, Meadows GG, et al. A novel approach to identify driver genes involved in androgen-independent prostate cancer. Mol Cancer 2014;13:120 doi 10.1186/1476-4598-13-120.
Pubmed: Author and Title
CrossRef: Author and Title
Google Scholar: Google Scholar Search

16. Sagredo AI, Sagredo EA, Cappelli C, Baez P, Andaur RE, Blanco C, et al. TRPM4 regulates Akt/GSK3-beta activity and enhances beta-catenin signaling and cell proliferation in prostate cancer cells. Mol Oncol 2018;12(2):151-65 doi 10.1002/1878-0261.12100.
Pubmed: Author and Title
CrossRef: Author and Title
Google Scholar: Google Scholar Search

17. Morrison BL, Mullendore ME, Stockwin LH, Borgel S, Hollingshead MG, Newton DL. Oxyphenisatin acetate (NSC 59687) triggers a cell starvation response leading to autophagy, mitochondrial dysfunction, and autocrine TNFalpha-mediated apoptosis. Cancer Med 2013;2(5):687-700 doi 10.1002/cam4.107.
Pubmed: Author and Title
CrossRef: Author and Title
Google Scholar: Google Scholar Search

18. Rajapakse VN, Luna A, Yamade M, Loman L, Varma S, Sunshine M, et al. CellMinerCDB for Integrative Cross-Database Genomics and Pharmacogenomics Analyses of Cancer Cell Lines. iScience

2018;10:247-64 doi 10.1016/j.isci.2018.11.029.
Pubmed: Author and Title
CrossRef: Author and Title
Google Scholar: Google Scholar Search

19. Mizunuma M, Redon CE, Saha LK, Tran AD, Dhall A, Sebastian R, et al. Acetalax (Oxyphenisatin Acetate, NSC 59687) and Bisacodyl Cause Oncosis in Triple-Negative Breast Cancer Cell Lines by Poisoning the Ion Exchange Membrane Protein TRPM4. Cancer Res Commun 2024;4(8):2101-11 doi 10.1158/2767-9764.CRC-24-0093.
Pubmed: Author and Title
CrossRef: Author and Title
Google Scholar: Google Scholar Search

20. Reinhold WC, Marangoni E, Elloumi F, Montagne R, Varma S, Wang Y, et al. Acetalax and Bisacodyl for the Treatment of Triple-Negative Breast Cancer: A Combined Molecular and Preclinical Study. Cancer Res Commun 2025;5(2):375-88 doi 10.1158/2767-9764.CRC-24-0435.
Pubmed: Author and Title
CrossRef: Author and Title
Google Scholar: Google Scholar Search

21. Luna A, Elloumi F, Varma S, Wang Y, Rajapakse VN, Aladjem MI, et al. CellMiner Cross-Database (CellMinerCDB) version 1.2: Exploration of patient-derived cancer cell line pharmacogenomics. Nucleic Acids Res 2021;49(D1):D1083-D93 doi 10.1093/nar/gkaa968.
Pubmed: Author and Title
CrossRef: Author and Title
Google Scholar: Google Scholar Search

22. Ohgane K, Yoshioka H. Quantification of gel bands by an ImageJ macro, Band/Peak Quantification Tool v1. Protocolsio 2019 doi 10.17504/protocols.io.7vghn3w.

23. Amin MB, Greene FL, Edge SB, Compton CC, Gershenwald JE, Brookland RK, et al. The Eighth Edition AJCC Cancer Staging Manual: Continuing to build a bridge from a population-based to a more "personalized" approach to cancer staging. CA Cancer J Clin 2017;67(2):93-9 doi 10.3322/caac.21388.
Pubmed: Author and Title
CrossRef: Author and Title
Google Scholar: Google Scholar Search

24. Sinha R, Luna A, Schultz N, Sander C. A pan-cancer survey of cell line tumor similarity by feature-weighted molecular profiles. Cell Rep Methods 2021;1(2):100039 doi 10.1016/j.crmeth.2021.100039.
Pubmed: Author and Title
CrossRef: Author and Title
Google Scholar: Google Scholar Search

25. Sevilla S, Sovacool K, Kuhn S, Tandon M, Koparda V. Rna sEquencing aNalysis pipElinE (v2.7.1). zenodo 2025(v2.7.1).

26. Dobin A, Davis CA, Schlesinger F, Drenkow J, Zaleski C, Jha S, et al. STAR: ultrafast universal RNA-seq aligner. Bioinformatics 2013;29(1):15-21 doi 10.1093/bioinformatics/bts635.
Pubmed: Author and Title
CrossRef: Author and Title
Google Scholar: Google Scholar Search

27. Liberzon A, Birger C, Thorvaldsdottir H, Ghandi M, Mesirov JP, Tamayo P. The Molecular Signatures Database (MSigDB) hallmark gene set collection. Cell Syst 2015;1(6):417-25 doi 10.1016/j.cels.2015.12.004.
Pubmed: Author and Title
CrossRef: Author and Title
Google Scholar: Google Scholar Search

28. Kohn KW, Zeeberg BM, Reinhold WC, Pommier Y. Gene expression correlations in human cancer cell lines define molecular interaction networks for epithelial phenotype. PLoS One 2014;9(6):e99269 doi 10.1371/journal.pone.0099269.

Pubmed: Author and Title
CrossRef: Author and Title
Google Scholar: Google Scholar Search

29. Arner E, Daub CO, Vitting-Seerup K, Andersson R, Lilje B, Drablos F, et al. Transcribed enhancers lead waves of coordinated transcription in transitioning mammalian cells. Science 2015;347(6225):1010-4 doi 10.1126/science.1259418.

Pubmed: Author and Title
CrossRef: Author and Title
Google Scholar: Google Scholar Search

30. Roper N, Velez MJ, Chiappori A, Kim YS, Wei JS, Sindiri S, et al. Notch signaling and efficacy of PD-1/PD-L1 blockade in relapsed small cell lung cancer. Nat Commun 2021;12(1):3880 doi 10.1038/s41467-021-24164-y.

Pubmed: Author and Title
CrossRef: Author and Title
Google Scholar: Google Scholar Search